

1 The changing mass of the Antarctic Ice Sheet during ENSO- 2 dominated periods in the GRACE era (2002-2022)

3 John Bright Ayabilah^{1,2}, Matt King^{1,2}, Danielle Udy², Tessa Vance³

5 ¹School of Geography, Planning, and Spatial Science, University of Tasmania, Hobart 7001, Tasmania, Australia

6 ²The Australian Centre for Excellence in Antarctic Science, Institute for Marine & Antarctic Studies, University
7 of Tasmania, Hobart 7001, Tasmania, Australia

8 ³Australian Antarctic Program Partnership, Institute for Marine & Antarctic Studies, University of Tasmania,
9 Hobart, TAS, 7001, Australia

10 *Correspondence to:* John Bright Ayabilah (johnbright.ayabilah@utas.edu.au)

13 **Abstract.** Large-scale modes of climate variability significantly influence Antarctic Ice Sheet (AIS) mass change.
14 Improved understanding of the relationship between these climate modes and AIS mass change can help reduce
15 uncertainties in future ice mass estimates and its contribution to sea level rise. However, the spatiotemporal
16 patterns of AIS mass variation driven by El Niño Southern Oscillation (ENSO)-induced atmospheric circulation
17 remain unclear. We investigated AIS mass variability during different ENSO periods using Gravity Recovery and
18 Climate Experiment (GRACE) observed mass changes and modelled surface mass balance (using RACMO2.4p1)
19 over the period 2002 to 2022. To allow comparison with GRACE, we used a cumulative sum indexing method to
20 define different ENSO-dominated ‘periods’ over 2002-2022. This method results in time periods that are
21 dominated by a particular phase of ENSO, that is not necessarily equivalent to specific events as derived from
22 canonical indices. The results show strong spatial variability in how the ENSO teleconnection cumulatively
23 manifests over the AIS. These differing spatial patterns are primarily driven by changes in the Amundsen Sea
24 Low strength, location, and extent, which alter circulation patterns and moisture flow in West Antarctica. In East
25 Antarctica, ice mass variability is largely influenced by the positioning of cyclonic and anticyclonic circulation
26 anomalies, primarily driven by the Southern Annular Mode; however, ENSO signals are also present. In both East
27 and West Antarctica, this study shows that the spatial impact of any given ENSO-dominant period can trigger
28 distinct circulation patterns which can variably influence surface mass balance and ice mass change. However,
29 uncertainties remain, as the mass variability observed during ENSO-dominant periods may not be solely attributed
30 to ENSO, due to teleconnections that may not have fully developed or may have been masked by other processes.

31 1. Introduction

32 The drivers of inter-annual to decadal Antarctic Ice Sheet (AIS) mass variability are complex and not yet fully
33 understood (IMBIE Team, 2018). External factors, such as episodic extreme precipitation events often linked to
34 atmospheric rivers (Wille et al., 2021), and internal factors, including ice dynamics (IMBIE Team, 2018), both
35 contribute to these variations. Understanding the mechanisms underlying AIS mass change and variability is
36 critical for improving future projections of ice mass changes and the Antarctic contribution to sea level rise.

37 The main determinants of the net AIS mass balance (MB) are ice discharge (D) from the continental margins of
38 Antarctica and Surface Mass Balance (SMB). SMB is further defined as accumulating precipitation and riming

39 onto the ice sheet, minus runoff, sublimation/evaporation and blowing snow erosion. The fluctuation of the AIS
40 mass balance and its subsequent contribution to sea level rise are based on the difference between ice discharge
41 and SMB (i.e., MB = SMB – D). The AIS SMB exhibits high variability on inter-annual to decadal timescales,
42 (Kim et al., 2020; Medley and Thomas, 2019; Van De Berg et al., 2006). Precipitation variability, driven by
43 atmospheric circulation, is a key determinant of Antarctic SMB and, over a wide range of timescales, including
44 interannual to decadal, is closely linked to modes of climate variability (Kim et al., 2020).

45 The Southern Annular Mode (SAM) is the dominant mode of extratropical variability in the Southern Hemisphere.
46 The SAM signal is driven by a combination of internal atmospheric dynamics and external forcings, including
47 stratospheric ozone depletion, increases in greenhouse gases, and tropical teleconnections (Fogt and Marshall,
48 2020a). It varies on timescales from weeks to decades, and its influence on Antarctic precipitation is regionally
49 dependent (Marshall et al., 2017). During the positive phase of SAM, the westerlies around 60° S strengthen, and
50 the overall impact on the AIS is a net decrease in SMB (Marshall et al., 2017; Medley and Thomas, 2019).
51 Conversely, the net influence of the negative phase of SAM on the AIS is an increase in SMB (Medley and
52 Thomas, 2019; Marshall et al., 2017). However, SAM related circulation patterns are not stationary and vary over
53 decades, meaning [that](#) the regional impacts may shift over time (Marshall et al., 2013).

54 The El Niño Southern Oscillation (ENSO) is the dominant mode of inter-annual climate variability globally (2–
55 7-year timescales) and is defined by variations in sea surface temperature (SST) anomalies in the tropical Pacific
56 (Mcphaden et al., 2006). The ENSO pathway to Antarctica is modulated by the Amundsen Sea Low (ASL), which
57 lies at the poleward end of a Rossby wave train originating in the tropics (Hoskins and Karoly, 1981). This Rossby
58 wave train leads to the formation of the Pacific South American mode 1(PSA-1), an atmospheric anomaly pattern
59 that enables ENSO signals to reach Antarctica (Hoskins and Karoly, 1981). This creates a positive pressure
60 anomaly over the Amundsen-Bellingshausen sector (ABS) during El Niño events—the positive phase of PSA-1
61 and negative pressure anomaly during La Niña conditions—the negative phase of PSA-1 (Turner, 2004; Hoskins
62 and Karoly, 1981). The ASL represents a climatological area of low pressure in the South Pacific and is a key
63 component of the nonzonal climatological circulation (Raphael et al., 2016a). The teleconnection between ENSO
64 and the ASL is strongest during the austral spring (September-November; SON) but exerts influence throughout
65 the year (Schneider et al., 2012; Clem and Fogt, 2013; Fogt et al., 2011). The strength, extent, and location of the
66 ASL shows significant variability during different ENSO phases and individual ENSO events, resulting in varying
67 atmospheric circulation patterns that strongly influences moisture and temperature distribution in West Antarctica
68 (Raphael et al., 2016a; Hosking et al., 2013). The impact of ENSO on Antarctic climate is modulated by the phase
69 of SAM, with the signal amplified when SAM and ENSO are atmospherically in phase (positive SAM/La Niña
70 or negative SAM/El Niño) and reduced when they are atmospherically out of phase (positive SAM/El Niño or
71 negative SAM/La Niña) (Clem et al., 2016; Fogt et al., 2011). Positive SAM and La Niña conditions are associated
72 with a deepening (i.e. lower pressure anomaly) ASL, while negative SAM and El Niño conditions weaken the
73 ASL, and influence its longitudinal shift (Raphael et al., 2016a; Hosking et al., 2013). The deepening of the ASL
74 induces continental wind outflow on its western flank, reducing precipitation and SMB over the Antarctic
75 Peninsula and from the Bellingshausen Sea to the Ross Sea region in West Antarctica, whereas a weakened ASL
76 leads to onshore winds that enhance precipitation and SMB (Zhang et al., 2021; Li et al., 2022). The longitudinal
77 shift of the ASL modifies these impact zones.

78 The spatial patterns and magnitude of AIS mass variability due to large-scale modes of climate variability remain
79 unclear. Studies on the role of ENSO in Antarctic climate have mostly focused on precipitation derived from
80 reanalysis products or modelled SMB data (e.g., Medley and Thomas, 2019; Clem et al., 2016; Clem and Fogt,
81 2013; Fogt et al., 2011). Only a few studies have examined the relationship between large-scale modes of climate
82 variability and recent observed ice mass variation using Gravity Recovery and Climate Experiment (GRACE)
83 observed AIS ice mass change time series on timescales ranging from months to decades (e.g., Bodart and
84 Bingham, 2019; Zhang et al., 2021; King et al., 2023). Most of these studies have focused on single strong ENSO
85 events, such as the 2015-2016 El Niño (Bodart and Bingham, 2019), or on the mean impact of ENSO on the AIS.
86 In contrast, our study investigates the spatial impacts of multiple individual ENSO periods (as defined in our
87 study), enabling an assessment of how AIS mass variability differs between events and capturing the diverse
88 responses across the ice sheet, rather than a mean [responsesignal](#).

89 The GRACE mission, launched in 2002, has contributed to our understanding of the redistribution of mass within
90 the Earth system, which is useful for observing changes of the Greenland and Antarctic ice sheets (Tapley et al.,
91 2004; Shepherd et al., 2012). GRACE-observed ice mass variability is related to atmospheric circulation-driven
92 snow accumulation and variation in ice discharge (Diener et al., 2021). Although mass loss from runoff and
93 sublimation is included in the GRACE signal, these components are relatively minor compared to discharge. Over
94 the interannual timescales, atmospheric variability dominates the observed mass changes (King et al. 2023).
95 Studies of ENSO's impact on AIS using GRACE-observed ice mass changes show that different ENSO events
96 result in varying climatic and surface weather effects, leading to different spatial patterns of AIS mass variability.
97 Bodart and Bingham (2019) demonstrated that during the 2015-2016 El Niño, the Antarctic Peninsula and West
98 Antarctica gained mass, while East Antarctica experienced a reduction in mass. This spatial pattern is also
99 consistent over a longer period, in line with Zhang et al. (2021) who found similar correlations. They observed a
100 bipolar spatial pattern: during El Niño events, there was a mass gain over the Antarctic Peninsula and West
101 Antarctica and a mass loss over East Antarctica, while the pattern reversed during La Niña events. The bipolar
102 spatial patterns are consistent with the results of King et al. (2023), based on a GRACE analysis for the period
103 2002-2021, and King and Christoffersen (2024), which used GRACE and altimetry data (2002-2020), despite
104 differences in approaches and study periods. However, other studies have suggested that specific ENSO events
105 and types of ENSO events have distinct impacts on Antarctic SMB that are not limited to a bipolar pattern (e.g.,
106 Macha et al., 2024; Sasgen et al., 2010).

107 This study aims to investigate the spatial patterns of ice mass change and the driving atmospheric circulation
108 conditions during various ENSO-dominated periods, as observed in GRACE-derived AIS mass variations
109 between 2002 and 2022. Since GRACE observes total mass change without distinguishing between the individual
110 components of the mass balance, we use SMB output from a regional climate model RACMO2.4p1 to assess the
111 contribution of SMB to the spatial patterns detected by GRACE. The results indicate that no two ENSO periods
112 have the same net effect on Antarctic ice mass, especially at regional scales, and the bipolar spatial pattern
113 observed in earlier studies is not consistent across all ENSO events. This variability suggests that the ENSO signal
114 in the AIS is shifted from its background pattern depending on event-specific atmospheric and oceanic factors.

115 **2. Data and Methods**

116 **2.1. AIS mass change**

117 We used the GRACE and GRACE Follow On data. [The data are](#) provided by the GFZ German Research Centre
118 for Geosciences (Landerer et al., 2020). The GRACE Follow-On mission, launched in May 2018, succeeded the
119 GRACE mission, which was decommissioned in October 2017 due to battery and fuel problems. This gap between
120 the GRACE and GRACE Follow-On missions resulted in the loss of data from July 2017 and May 2018. Our
121 analysis involved GRACE data spanning from April 2002 to Dec 2022 without gap filling. We used the COST-G
122 release 1 version 3 (RL-01 V0003) gridded mass anomaly product, which combines GRACE/GRACE-FO
123 solutions from multiple GRACE analysis centres (Landerer et al., 2020). The data [are](#) provided on 50 km grid
124 products with approximately monthly temporal sampling. However, GRACE data have an underlying spatial
125 resolution of ~300km (Sasgen et al., 2020; Dahle et al., 2024). This relatively coarse resolution limits GRACE's
126 ability to resolve or capture relatively small mass changes, particularly those associated with localised SMB
127 anomalies.

128 The various available GRACE data products differ based on the processing methods and background models used.
129 The gridded mass change product adopted here is initially derived by solving for spherical harmonic coefficients
130 and then computing mass anomalies for each grid cell across the entire ice sheet using tailored sensitivity kernels
131 that minimise both GRACE and leakage error (Groh and Horwath, 2016). Within this product, glacial isostatic
132 adjustment is corrected using the ICE6G_D model (Peltier et al., 2018), although this has no bearing on non-linear
133 variability as studied here. [The effects of atmospheric and oceanic effects on mass redistribution are modelled](#)
134 [using standard de-aliasing products. are also modelled in a similar fashion to as are s](#)pherical harmonic degree-1
135 [terms are added, i.e.](#) based on the approach of Swenson et al. (2008). Further details about the GRACE time
136 series, post-processing techniques, and quality assessment can be found in Dahle et al. (2019). It is worth noting
137 that the GRACE-observed ice mass change time series is affected by systematic errors associated with the GRACE
138 orbital geometry and small unmodelled errors, evident in the (largely north-south) striping pattern observed in
139 some of the ice mass change results.

140 We focus our analysis on the ENSO signal in ice mass variation during different ENSO-dominated periods. First,
141 we removed short-term signal fluctuations in the GRACE data by applying a 7-month moving median smoother
142 to the GRACE time series. This filter choice, following King et al. (2023), is a subjective decision aimed at
143 dampening month-to-month noise without distorting longer-term variability. Since our focus is on GRACE-
144 observed ice mass variability, we subtracted the linear trend at each grid point, estimated using ordinary least
145 squares over the data span. This effectively produces mass anomalies with respect to the [climatology of the](#)
146 [entire 2002–2022](#) GRACE period.

147 To understand the relationship between ice mass changes and ENSO-dominated periods, we computed the rate of
148 ice mass change for each identified ENSO-dominated period. These rates represent the impact of ENSO during
149 each ENSO-dominated period. We calculated the rates for each grid cell of the gridded GRACE ice mass anomaly
150 data and generated spatial patterns of ice mass trends for each ENSO-dominated period.

151 **2.2. Climate indices**

152 To characterise ENSO variability, we used the Niño3.4 index, one of several metrics that measures the strength
153 and phase of ENSO based on [sea-surface temperature SST](#) anomalies in the central and eastern tropical Pacific.
154 This index is obtained by tracking the running five-month mean SST based on the HadISST record over 5°N–5°S,
155 170°W–120°W (Rayner et al., 2003) and is normalised and shown in Fig. 1a. It is provided by the Climate
156 Prediction Centre (CPC) of the National Oceanic and Atmospheric Administration (NOAA) and can be accessed
157 at <https://psl.noaa.gov/data/timeseries/month/Nino34/>. The Niño3.4 temperature anomalies are standard for
158 detecting and monitoring ENSO events but cannot differentiate between eastern and central ENSO events. We
159 used the Niño3.4 index because our focus was on the spatial variability in AIS mass during all ENSO events,
160 rather than differentiating between eastern and central ENSO events.

161 For SAM, we used the station-derived index from Marshall (2003), available at <http://www.nerc-bas.ac.uk/icd/gjma/sam.html>, and shown in Fig. 1a. This index is based on the zonal pressure differences at 12
162 stations located between 40 °S and 65 °S.

164 To identify ENSO signatures in the GRACE data, we first identified El Niño- and La Niña-dominated periods
165 based on the cumulative summed indices, which act as a sort of low-pass filter of the raw indices. The cumulative
166 summed indices were derived from anomalies relative to their climatological mean using a reference window of
167 1971–1999. This period is a well observed period before the commencement of GRACE and is the same as that
168 chosen by King et al. (2023). After the indices were normalised using the mean and standard deviation computed
169 within the reference window, the normalised indices were restricted to the GRACE period, cumulatively summed,
170 detrended, and renormalised.

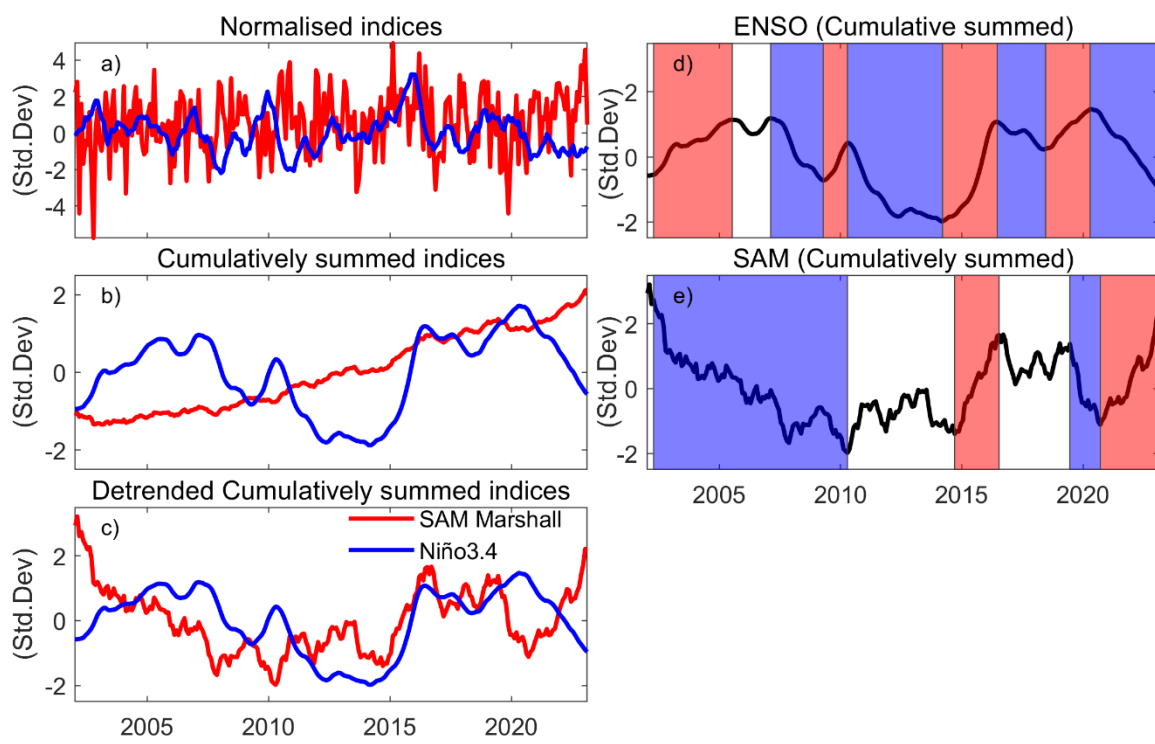
171 To investigate the potential linkage between large-scale climate variability and ice mass variation, we
172 cumulatively summed all the climate indices (Fig 1b) and [further](#) detrended [them](#) (Fig. 1c). The AIS mass reflects
173 the compound effect of surface mass fluxes over time. The cumulative mass flux observed by GRACE reflects
174 the cumulative climate indices (King et al., 2023) as opposed to raw indices, which relate to mass flux. These
175 cumulative indices are also captured by modelled cumulative SMB (Kim et al., 2020; Diener et al., 2021). The
176 alternative approach is to difference GRACE data in time, but this inflates the GRACE noise and reduces the
177 lower frequency signal and is hence undesirable (King et al., 2023).

178 In this study, we defined El Niño-dominated periods as intervals during which the positive phase of ENSO persists
179 and outweighs the negative phase, culminating in a positive peak in the cumulative ENSO index. Similarly, La
180 Niña-dominated periods are defined as intervals during which negative phase outweighs the positive phase,
181 culminating in a negative peak. Only ENSO periods with a minimum duration of 12 months were considered in
182 our analysis. In a cumulatively summed index, these are expressed as sustained periods of positive (El Niño) or
183 negative (La Niña) slope. Based on this criterion, we identified four El Niño-dominated periods over the GRACE
184 time steps: 2002–2005, 2009–2010, 2014–2016, and 2018–2020 (Fig. 1d). An equal number of La Niña-dominated
185 periods were found, covering 2007–2009, 2010–2014, 2016–2018, and 2020–2022. The strength of the expression
186 of the ENSO signal in the Antarctic climate is modulated by the phase of SAM (Fogt et al., 2011). During the
187 2002–2005 El Niño-dominated period, the cumulative SAM index was dominated by negative SAM until around

188 2008 (atmospherically in phase El Niño/-SAM). After 2008, the cumulative SAM index exhibited no notable
 189 trend, indicating a neutral phase. During the 2014-2016 El Niño, cumulative SAM and ENSO indices were
 190 atmospherically out of phase (El Niño/+SAM). SAM shifted to a neutral state during the 2016-2018 La Niña.
 191 SAM and ENSO were atmospherically in phase during the 2018-2020 El Niño (El Niño/-SAM) and 2020-2022
 192 La Niña (La Niña/+SAM), which is notable as the only time positive SAM and La Niña co-occurred over the
 193 GRACE period (Fig. 1d, e).

194 Note that we do not distinguish between Central Pacific (CP) and Eastern Pacific (EP) El Niño events in our
 195 analysis because our ENSO dominated periods frequently span multiple years. Indeed, examining the cumulative
 196 CP and EP indices shows they are very similar, aside from 2016-2018, and hard to distinguish in an analysis of
 197 GRACE data (Supplementary Fig. S1b). Our method using the Niño3.4 index encapsulates variations in the
 198 tropical spatial pattern of SST anomalies.

199
 200



201
 202 **Figure 1. Monthly climate indices of SAM (Marshall, 2003) and Niño3.4 from 2002-2022:** (a) normalised
 203 SAM and Niño3.4 indices; (b) normalised cumulatively summed SAM and Niño3.4 indices; (c) detrended,
 204 cumulatively summed SAM and Niño3.4 indices (normalised). Periods until positive and negative peaks
 205 are reached in the cumulatively summed Niño3.4 are defined as El Niño-dominated and La Niña-
 206 dominated periods, respectively, represented as red and blue shaded areas in (d). Similarly, periods until
 207 positive and negative peaks are reached in the cumulatively summed SAM index (Marshall, 2003) are
 208 defined as SAM-positive and SAM-negative dominated periods, respectively, denoted as red and blue
 209 shaded areas in (e). Neutral dominated periods are represented by white shading.

210 **2.3. SMB model outputs**

211 We used modelled SMB output from the Regional Atmospheric Climate Model RACMO2.4p1 model ([Van Dalum](#)
212 [et al., 2025; Van Dalum et al., 2024](#)). This model has a horizontal resolution of 11 km and a vertical resolution of
213 40 atmospheric levels. This version of SMB model output is forced by ERA5 reanalysis data at its lateral
214 boundaries and SST and sea ice extent at the sea surface boundary, with data available from 1979 onward.
215 Compared with previous releases, RACMO2.4p1 provides a better representation of SMB process which agree
216 with observation (Van Dalum et al., 2025; Van Dalum et al., 2024). For our study, monthly SMB values truncated
217 to the GRACE period were used, covering Apr 2002 to Dec 2022. To compare with GRACE data, we computed
218 anomalies relative to the 2002-2022 mean and then cumulatively summed them to obtain cumulative SMB
219 anomalies in units of kg m^{-2} . These anomalies were then interpolated to match the GRACE grid spacing and time
220 steps. We detrended the cumulative SMB and performed a regression analysis on these anomalies for each defined
221 ENSO-dominated period.

222 **2.4. Reanalysis climate data**

223 To explore the potential climatic forcing during an ENSO-dominated period, we examined monthly mean ERA5
224 reanalysis model 10 m winds and sea level pressure from 2002 to 2022, with a resolution of 0.25° by 0.25°
225 (Hersbach et al., 2020). Anomalies of 10 m zonal and meridional wind components, as well as sea level pressure,
226 were computed for each grid cell relative to the mean over the GRACE period, for all regions south of 40° S. We
227 then computed anomaly composite means for each ENSO-dominated period. We used ERA5 products instead of
228 RACMO outputs because ERA5 provides broader spatial coverage and is more suitable for capturing large-scale
229 atmospheric circulation patterns, which are critical for analysing ENSO-related teleconnections. Additionally,
230 RACMO is forced by ERA5.

231 **2.5. Definitions of events, periods and anomaly interpretations used in this study**

232 [We acknowledge that we use multiple terminologies in this study to define both our results, and when comparing](#)
233 [to the literature. For example, we use the term ‘El Niño- or La Niña-dominated period’ or simply ‘period’](#)
234 [to when considering the periods of time of sustained ENSO phase we as defined using our cumulatively](#)
235 [summed index. In contrast, when comparing to or describing other literature, we use the term ‘El Niño/ La Niña](#)
236 [event’ which refers to the peak phase of ENSO events. We also describe anomalies from the mean over the](#)
237 [GRACE period. For the purposes of this study, the pressure and wind fields, as well as SMB and GRACE mass](#)
238 [change, depicted in the figures represent anomalies from the \[climatology 2002–2022 period\]\(#\) for each relevant](#)
239 [variable. That is, for a given wind and pressure map, the fields depict wind and pressure anomalies against the](#)
240 [2002-2022 mean \(the GRACE data period\). For example, positive anomalies over the Antarctic continent reflect](#)
241 [a relative strengthening of the mean Antarctic High, while negative anomalies reflect a relative weakening of the](#)
242 [Antarctic High \(not the presence of a low\). For SMB, positive SMB and GRACE anomalies represent an increase](#)
243 [in mass, whereas negative anomalies indicate a reduction in mass relative to \[the 2002–2022 climatology\]\(#\).](#)

244 **2.6. Statistical significance of the results**

245 To quantify the significance of our regression trends at each grid point, we employed a two-tailed Student’s t-test.
246 The standard error of the slope at each grid point was calculated from the regression residuals and used to assess

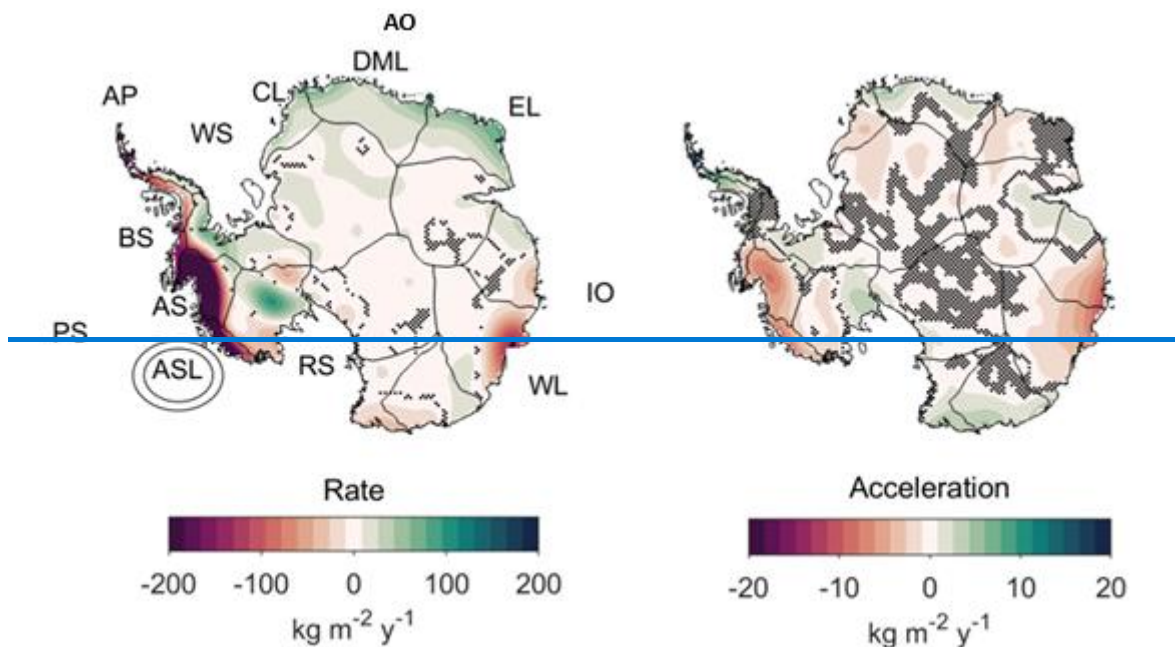
247 whether the slope significantly differed from zero at the 5% significance level. For mean sea level pressure
248 anomaly composites, statistical significance was assessed [relative to the 2002–2022 based on deviations from the](#)
249 [climatological](#) baseline using a two-sample *t*-test assuming unequal variances, also at the 5% significance level.

250 **3. Results**

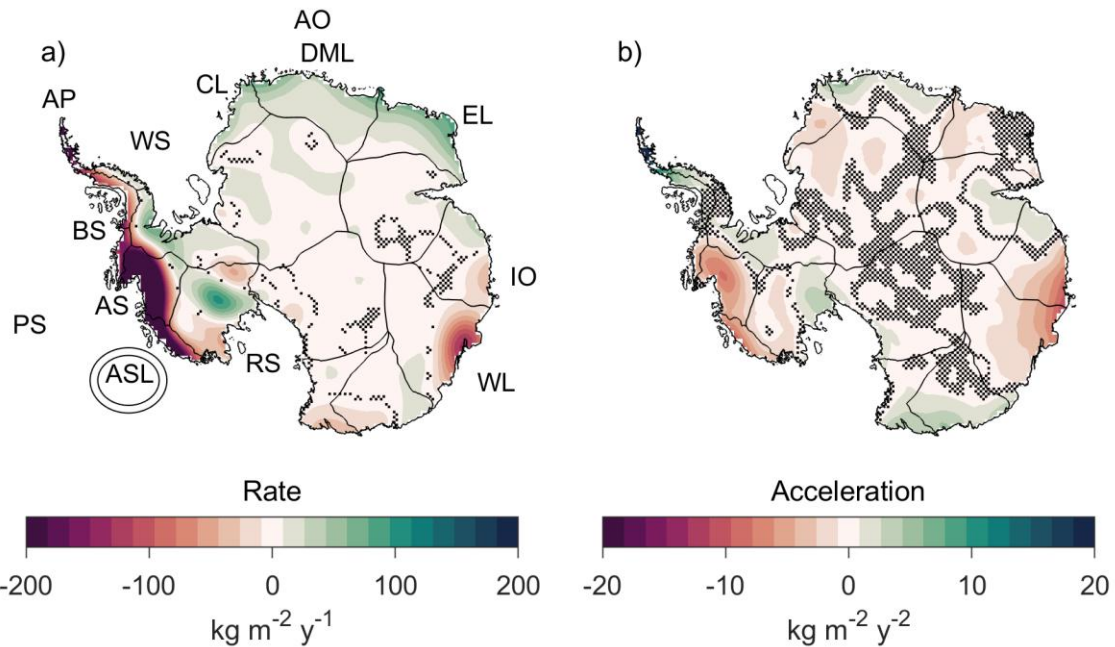
251 **3.1 Ice mass change**

252 We start by examining the long-term trend and acceleration in AIS mass change over the GRACE observational
253 period, represented by the linear and quadratic terms in the regression, respectively (Fig. 2). The spatial pattern
254 reveals strong regional variability, with areas of both positive and negative mass anomalies. While not identical,
255 the linear rate and acceleration exhibit closely aligned spatial patterns of mass change. In West Antarctica, the
256 rate of ice mass loss is most pronounced in the Amundsen Sea and Bellingshausen Sea sectors, where accelerated
257 ice discharge is well documented (Rignot et al., 2019; Gardner et al., 2018). The East Antarctic ice sheet shows
258 mass gain across Dronning Maud Land (and through to Enderby Land); conversely, the Wilkes Land sector has
259 experienced a decline in mass. The negative acceleration observed in the Amundsen Sea sector and Wilkes Land
260 indicates that the rate of mass loss in these regions is increasing over time.

261 While the long-term trend in AIS mass is primarily driven by ice dynamics, the interannual variability is more
262 closely linked to changes in precipitation (Kim et al., 2020). Short-term mass fluctuations can be influenced by
263 large-scale circulation modes. To explore the impact of ENSO on ice mass variability, we next examine how
264 atmospheric circulation and mass anomalies respond to ENSO forcing.



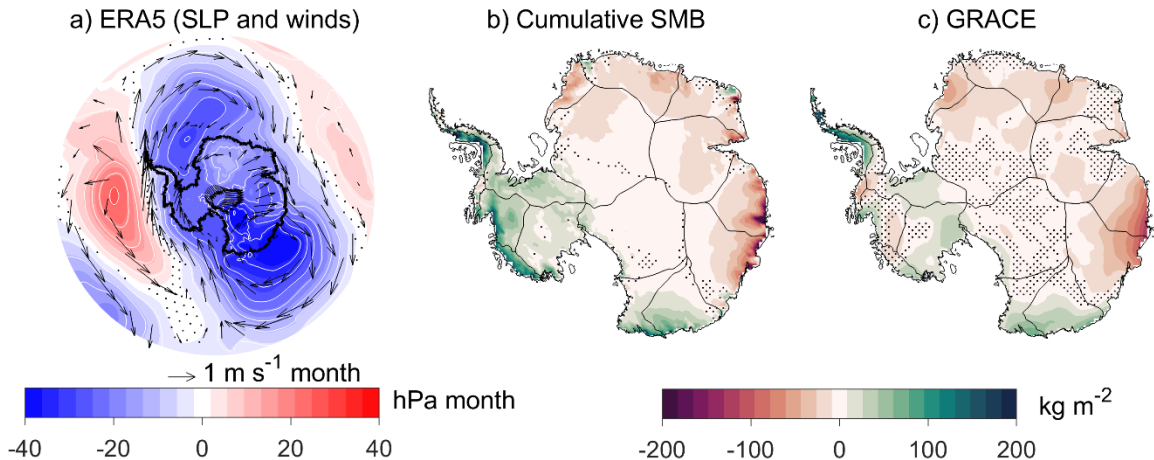
265



266

267 **Figure 2. a) Linear rate and b) acceleration of AIS mass change (2002-2022) based on GRACE data from**
 268 **using univariate regression. Key Antarctic regions are labelled: Antarctic Peninsula (AP), Bellingshausen**
 269 **Sea (BS), Amundsen Sea (AS), Amundsen Sea Low (ASL), Pacific Sector (PS), Ross Sea (RS), Indian**
 270 **Ocean (IO), Atlantic Ocean (AO), Wilkes Land (WL), Enderby Land (EL), Dronning Maud Land (DML)**
 271 **, Coats Land (CL), and Weddell Sea (WS). Stippling indicates areas not statistically significant ($p \geq 0.05$).**
 272 **Significance tests do not reflect the effects of temporal correlations in these data (Williams et al., 2014).**

273 Figure 3 presents the regression results of cumulatively summed anomalies in ERA5 reanalysis climate variables
 274 (sea level pressure and 10 m winds) and RACMO2.4p1 model SMB, along with GRACE-derived ice mass change
 275 anomalies, against the cumulatively summed Niño3.4 index. All variables were detrended before regression to
 276 focus on the variability. The results show that the cumulative ENSO is associated with shifts in atmospheric
 277 circulation that supports the observed dipole SMB and ice mass anomaly between West and East Antarctica (Fig.
 278 3a)



279 **Figure 3. Maps show the regression of cumulatively summed sea level pressure (shaded region and**
 280 **contour) and 10 m wind anomalies (represented by reference vectors (m s^{-1}) from ERA5 reanalysis (a),**
 281 **cumulatively summed RACMO2.4p1 model SMB anomalies (b), and GRACE ice mass change anomalies**
 282 **(c) regressed against cumulatively summed Niño3.4. The u and v wind components were regressed**
 283 **separately. All panels reflect regression anomalies over the period 2002-2022. All variables were linearly**
 284 **detrended prior to regression using the full data periods. Stippling indicates regions where the regression**
 285 **results are not statistically significant ($p \geq 0.05$).**

287 We also compared the regression results presented in Figure 3 with El Niño and La Niña composites (see
 288 [supplementary](#) Fig. S2) derived from annual accumulated SMB anomalies and annual mean Niño3.4 index, which
 289 broadly agree with the cumulative approach spatial patterns observed in West and East Antarctica. From the
 290 composite map ([supplementary](#) Fig. S2, covering 2002-2022), we observe that in West Antarctica, El Niño years
 291 are associated with a positive mean SMB anomaly ($26.98 \text{ kg m}^{-2} \text{ yr}^{-1}$), while La Niña years correspond to a
 292 negative mean anomaly ($-10.29 \text{ kg m}^{-2} \text{ yr}^{-1}$). In contrast, East Antarctica shows a negative mean SMB anomaly
 293 ($-3.14 \text{ kg m}^{-2} \text{ yr}^{-1}$) during El Niño years and a positive anomaly ($5.28 \text{ kg m}^{-2} \text{ yr}^{-1}$) during La Niña years.

294 Our result shows that, spatially, SMB and ice mass [increases](#) in West Antarctica and decrease in East Antarctica
 295 during El Niño-dominated periods, with the pattern reversing during La Niña-dominated periods (Fig. 3b–c). The
 296 cumulative ENSO-induced changes in meridional flow are associated with the SMB variability (Fig. 3a–b). Since
 297 [changes in](#) SMB [fluctuations](#) are closely linked to ice mass change, the spatially coherent patterns between SMB
 298 and GRACE-derived ice mass change [vary](#) (Fig. 3b–c).

299 However, in West Antarctica, the SMB signal differs from GRACE-derived ice mass changes, which indicate [s](#)
 300 relatively modest positive mass anomalies compared to the stronger SMB signal (Fig. 3b–c), whereas in East
 301 Antarctica, the two signals are more closely aligned.

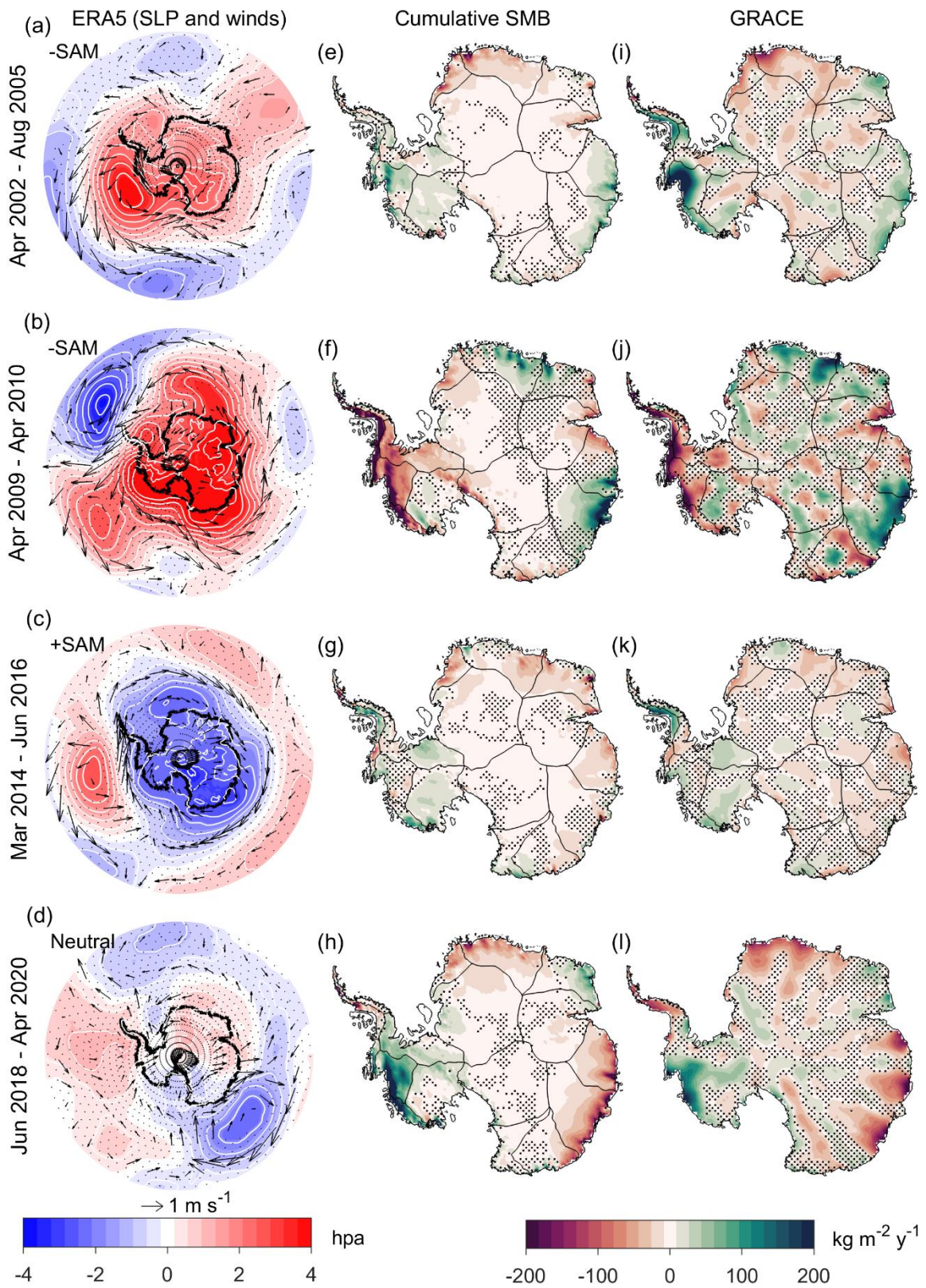
302 We next focus on the variability within ENSO-dominated periods and find that no two ENSO periods are identical.
 303 We examine AIS mass change, SMB variability, and the atmospheric circulation driving these changes during
 304 different ENSO-dominated periods we defined in this study (see section 2.2). The results reveal distinct spatial

305 patterns of ice mass change associated with individual El Niño and La Niña events. We remind the reader that the
306 GRACE signal is more reliable in the coastal regions and less reliable in the interior, where inherent systematic
307 errors in GRACE measurements in the form of north-south striping are more pronounced.

308 **3.2. El Niño-dominated periods**

309 Across the Antarctic continent, spatial pressure anomalies vary between El Niño-dominated periods, with both
310 positive and negative pressure anomalies observed (Fig. 4a–d). These pressure patterns reflect either a relative
311 intensification or relative weakening of the mean Antarctic High (Fig. 4a–b). These variations align with the
312 cumulatively summed SAM indices (Fig. 1e), where high-pressure anomalies correspond to prolonged negative
313 SAM phases, and low-pressure anomalies coincide with prolonged positive SAM phases. Mass anomalies
314 observed in both RACMO SMB and GRACE are most pronounced along the coastal regions, where the signals
315 are statistically significant. In this study, we focus on the absolute mass changes during each period, while relative
316 impacts are presented in [the supplement](#) (Fig. S3).

El Niño-dominated periods



318 **Figure 4. Atmospheric circulation anomalies relative to the GRACE period (2002–2022) (a–d^{left}), rate of**
319 **change in cumulative SMB anomalies from RACMO2.4p1 model (e–h^{middle}) and linear rate of GRACE–**
320 **derived ice mass anomalies (i–l^{right}) during El Niño-dominated period. Sea level pressure anomalies are**
321 **shown as shaded regions with contours (hPa), while wind anomalies are indicated by reference vectors**
322 **(m s^{−1}). SMB and GRACE maps (kg m^{−2} y^{−1}) illustrate variability in AIS mass for each identified El Niño–**
323 **dominated period. The GRACE signal is more reliable in the coastal regions and less reliable in the**
324 **interior, where GRACE systematic error in the form of north-south striping is more evident. Non-**
325 **significant areas are stippled for the pressure anomalies and AIS mass trend at p-value ≤ 0.05 .**

326 3.2.1. West Antarctic anomalies during El Niño-dominated periods

327 In West Antarctica, El Niño-dominated periods are characterised by a positive pressure anomaly in the Pacific
328 sector off the West Antarctic coastline (Fig. 4a–b). The position and strength of these positive pressure anomalies
329 vary for each El Niño-dominated period, which is also reflected in the variation of wind anomalies and spatial
330 patterns of SMB (Fig. 4e–h) and ice mass change (Fig. 4i–l). However, during the 2018–2020 period, no
331 significant pressure anomaly is observed, and in the 2009–2010 period, a significant pressure anomaly is located
332 closer to the continent, with a non-significant pressure anomaly further north (Fig. 4a–b).

333 During three out of four El Niño-dominated periods (2002–2005, 2014–2016, and 2018–2020), the Amundsen
334 Sea sector shows positive anomalies in both SMB (Fig. 4e, g–h) and ice mass anomalies (Fig. 4i, k–l), indicating
335 mass gain, despite variations in the location and strength of the positive pressure anomaly in the Pacific (Fig. 4a,
336 c–d). The positive mass anomalies are more widespread across the Amundsen Sea sector during the 2002–2005
337 period in GRACE (Fig. 4i) and in both SMB and GRACE during the 2018–2020 period (Fig. 4h, l). The positive
338 pressure anomaly in the Pacific which supports these mass gains, is significant during the 2002–2005 period.

339 For the 2014–2016 El Niño-dominated period, we observed weak and, in some regions, non-significant positive
340 SMB and ice mass anomalies in the Amundsen Sea sector and western Ross Sea (Fig. 4g, k). During this period,
341 our cumulative ENSO and SAM were out of phase (El Niño/+SAM), as evidenced by significant negative pressure
342 anomalies over the continent (Fig. 4c). The positive pressure anomaly in the Pacific was located away from the
343 coastline and was associated more with wind anomalies along the shore, rather than onshore (Fig. 4c).

344 The mass change pattern in the Amundsen Sea sector during the 2009–2010 El Niño-dominated period is distinct
345 from the other El Niño periods, with widespread significant negative SMB (Fig. 4f) and ice mass (Fig. 4j)
346 anomalies indicating a net mass reduction. In contrast to the other El Niño periods, a large area of significant
347 positive pressure anomaly extends offshore from the Antarctic continent, spanning from the Peninsula to beyond
348 the Ross Sea, and supports offshore wind anomalies in the Amundsen Sea sector (Fig. 4b).

349 The Antarctic Peninsula exhibits contrasting mass change responses during El Niño-dominated periods (Fig. 4).
350 Positive SMB (Fig. 4e, g) and ice mass anomalies (Fig. 4j, l) are observed during the 2002–2005 and 2014–2016
351 El Niño periods, particularly in GRACE (Fig. 4i, k), whereas negative SMB (Fig. 4f, h) and ice mass anomalies
352 (Fig. 4j, l) are evident during the 2009–2010 and 2018–2020 periods. These mass change pattern align with
353 pressure anomaly distributions and are associated with onshore wind anomalies during the 2002–2005 and 2014–

354 2016 periods (Fig. 4a, c) and offshore wind anomalies for 2009–2010 and 2018–2020 (non-significant) periods
355 (Fig. 4b, d).

356 **3.2.2. East Antarctic anomalies during El Niño dominated periods**

357 In the Atlantic Ocean sector, three out of four El Niño-dominated periods (2002–2005, 2014–2016, and 2018–
358 [show](#) consistent [patterns](#) with negative SMB (Fig. 4e, g–h) and ice mass (Fig. 4i, k–l) anomalies in Dronning
359 Maud Land. The reduction in mass is more extensive during the 2002–2005 and 2018–2020 El Niño periods,
360 covering much of Coats Land and Dronning Maud Land, with strong mass anomalies along the western edge of
361 Dronning Maud Land (Fig. 4e, h, i, l). The magnitude of mass reduction is lesser for the 2014–2016 El Niño
362 period (Fig. 4g). However, among these periods, the 2014–2016 El Niño period shows a significant pressure
363 anomaly, which can be directly associated with the observed mass reduction patterns.

364 Conversely, during the 2009–2010 El Niño period, we observed a significant anomalous mass gain in Dronning
365 Maud Land (Fig. 4f, j). This mass gain coincides with a significant positive pressure anomaly over the Atlantic,
366 which supports onshore wind anomalies into Dronning Maud Land.

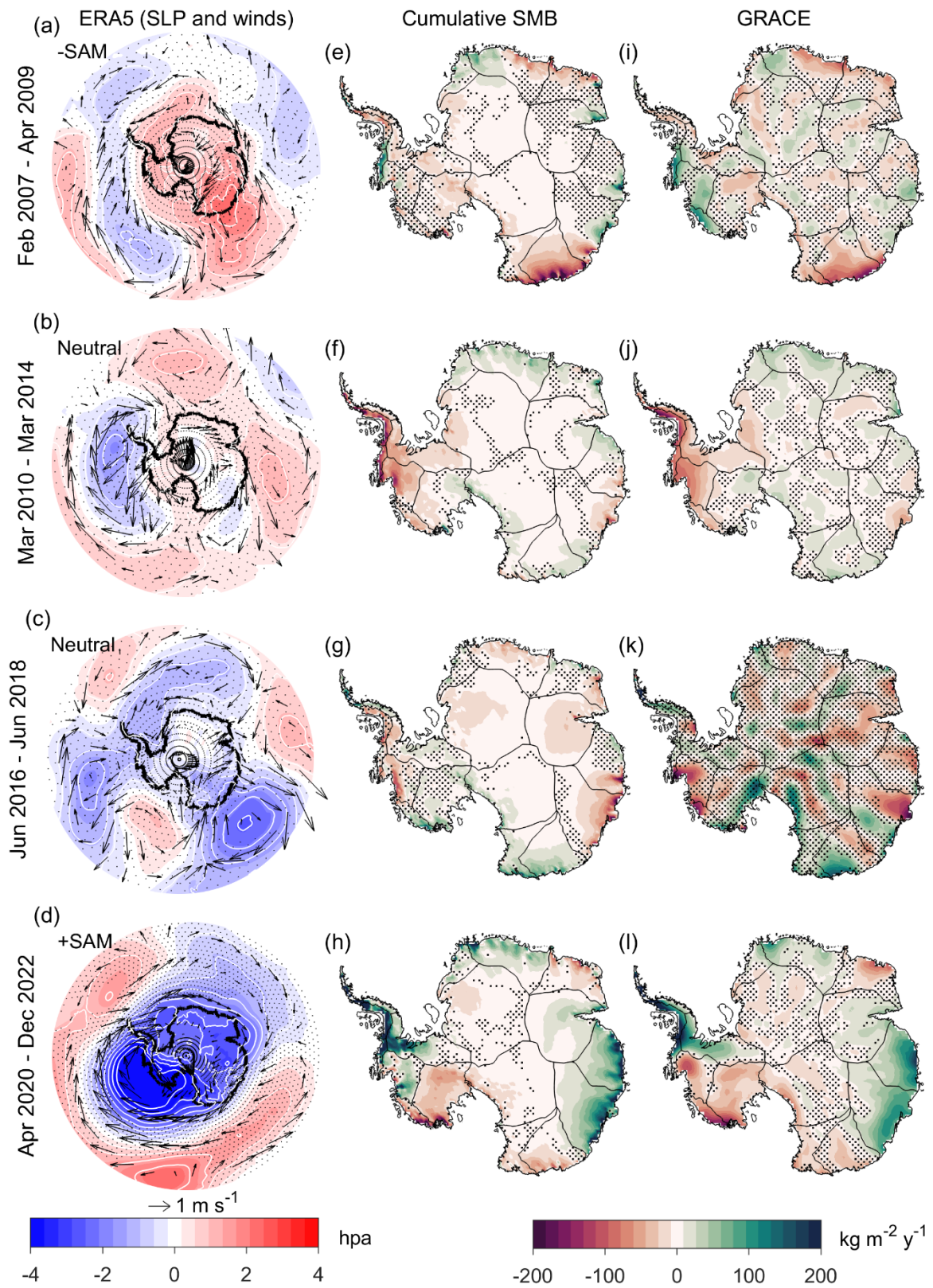
367 Enderby Land shows positive mass anomalies, which in some instances are evident in GRACE but not in SMB,
368 and vice versa. For example, during the 2002–2005 El Niño period, positive mass anomalies are more pronounced
369 in GRACE than in SMB (Fig. 4e, i), whereas during the 2018–2020 El Niño period, the positive anomalies are
370 stronger in SMB than in GRACE (Fig. 4h, l). Atmospheric circulation anomalies during the 2009–2010 and 2014–
371 2016 El Niño periods are statistically significant and supports the observed mass change patterns. For the 2002–
372 2005 and 2018–2020 El Niño periods, we cannot associate the observed mass patterns to circulation anomalies at
373 the 0.05 significance level.

374 In the Indian Ocean sector/Wilkes Land, mass gain is broadly observed during the 2002–2005 and 2009–2010 El
375 Niño periods (Fig. 4e–f, i–j), and a reduction in mass during the 2014–2016 and 2018–2020 El Niño periods (Fig.
376 4g–h, k–l). During the periods with mass gain, positive pressure anomalies were present over Wilkes Land (Fig.
377 4a–b), with the anomaly more intense and statistically significant during the 2009–2010 El Niño period and
378 associated with a greater magnitude of mass gain in Wilkes Land (Fig. 4b, f, j). Conversely, during periods broadly
379 associated with mass reduction (Fig. 4g–h, k–l), negative pressure anomalies were observed around the Wilkes
380 Land region, aligned with offshore wind anomalies across much of the sector (Fig. 4c–d).

381 **3.3. La Niña-dominated periods**

382 Figure 5 presents atmospheric circulation patterns, SMB anomalies, and AIS mass changes during La Niña-
383 dominated periods. Absolute mass changes are shown in this section, while relative mass changes can be found
384 in [the supplementary material](#) (Fig. S43). The atmospheric circulation pattern anomalies during La Niña-
385 dominated periods (Fig. 5a–d) shows fewer areas of statistical significance compared to the El Niño periods (Fig.
386 4a–d). Instrument malfunctions and the termination of the GRACE mission in 2017 introduced noise and data
387 gaps, affecting ice mass estimates. Therefore, we limit our discussion to the atmospheric circulation and SMB for
388 the 2016–2018 La Niña-dominated period to avoid conclusions based on potentially unreliable data in GRACE.

La Niña-dominated periods



390 **Figure 5. Atmospheric circulation anomalies relative to the GRACE period (2002–2022) (a–d^{left}), rate of**
391 **change in cumulative SMB anomalies from the RACMO2.4p1 model (e–h^{middle}), and linear rate of**
392 **GRACE-derived ice mass anomalies (i–l^{right}) during La Niña-dominated period. Sea level pressure**
393 **anomalies are shown as shaded regions with contours (hPa), 10 m wind anomalies are indicated by**
394 **reference vectors (m s^{−1}). SMB and GRACE (kg m^{−2} y^{−1}) maps illustrate variability in AIS mass for each**
395 **identified La Niña-dominated period. The GRACE signal is strongest near the coastal regions and weaker**
396 **in the interior, where uncertainties are higher. The GRACE satellite malfunction during 2016–2018 is**
397 **apparent in the signal for that period, where instrument noise dominates over actual variability with**
398 **pronounced north-south striping. Non-significant areas are stippled for the pressure anomalies and AIS**
399 **mass trend at p-value ≥ 0.05 .**

400 **3.3.1. West Antarctic anomalies during La Niña-dominated periods**

401 Overall, during our La Niña-dominated periods, the Pacific sector exhibits a persistent negative pressure anomaly
402 (Fig. 5a–d), which appears more elongated than the positive pressure anomaly associated with El Niño periods.
403 This pressure anomaly is statistically significant for the 2020–2022 La Niña period; however, there are also
404 significant regions near the centre of the pressure anomaly during the 2010–2014 La Niña period.

405 Three out of the four La Niña periods (2010–2014, 2016–2018, and 2020–2022) are broadly associated with
406 negative SMB (Fig. 5f–h) and ice mass anomalies (Fig. 5j–l) across the Amundsen Sea sector. The reduction in
407 mass during the 2020–2022 and 2010–2014 La Niña periods aligns with a significant negative pressure anomaly
408 in the Pacific sector, and offshore wind anomalies (Fig. 5b, d).

409 In contrast, during the 2007–2009 La Niña period, a mass gain is prominently observed in GRACE (Fig. 5i), a
410 pattern more commonly associated with El Niño periods described earlier. However, the SMB and pressure
411 anomaly patterns during this period are not statistically significant at the 0.05 level.

412 Similar to the Amundsen Sea sector, the Antarctic Peninsula exhibits contrasting mass change responses during
413 La Niña-dominated periods. Broadly, negative mass anomalies are observed during the 2007–2009 and 2010–
414 2014 La Niña periods (Fig. 5i–j), whereas positive mass anomalies are evident during the 2016–2018 and 2020–
415 2022 La Niña periods (Fig. 5k–l). The magnitude of mass reduction is strongest during the 2010–2014 La Niña
416 period, while the mass gain is most pronounced during the 2020–2022 La Niña period.

417 This contrasting mass change response between the two periods aligns with the position of the negative pressure
418 anomaly in the Pacific sector. In the 2010–2014 La Niña period, the pressure anomaly is centred over the
419 Bellingshausen Sea, accompanied by offshore wind anomalies over the Peninsula (Fig. 5b). In contrast, during
420 the 2020–2022 La Niña period, the negative pressure anomaly is centred in the Amundsen Sea, with onshore wind
421 anomalies directed into the Peninsula (Fig. 5d).

422 **3.3.2. East Antarctic anomalies during La Niña-dominated periods**

423 Along the Atlantic sector, a dipole-like mass anomaly pattern is present during the 2007–2009 and 2020–2022 La
424 Niña periods (Fig. 5e, h), whereas a more uniform response is observed during the 2010–2014 and 2016–2018 La
425 Niña periods (Fig. 5f–g). During the 2007–2009 La Niña period, positive SMB anomalies were observed over

426 Coats Land and negative SMB anomalies toward Enderby Land (Fig. 5e), with this spatial pattern reversed during
427 the 2020–2022 La Niña period (Fig. 5h).

428 Positive mass anomalies were also observed across the Atlantic region during the 2014–2016 La Niña period,
429 with a reversed pattern during the 2016–2018 La Niña period (Fig. 5f–g). Regionally, Dronning Maud Land shows
430 consistent positive SMB (Fig. 5f, h) and ice mass anomalies (Fig. 5j, l) during the 2010–2014 and 2020–2022 La
431 Niña periods.

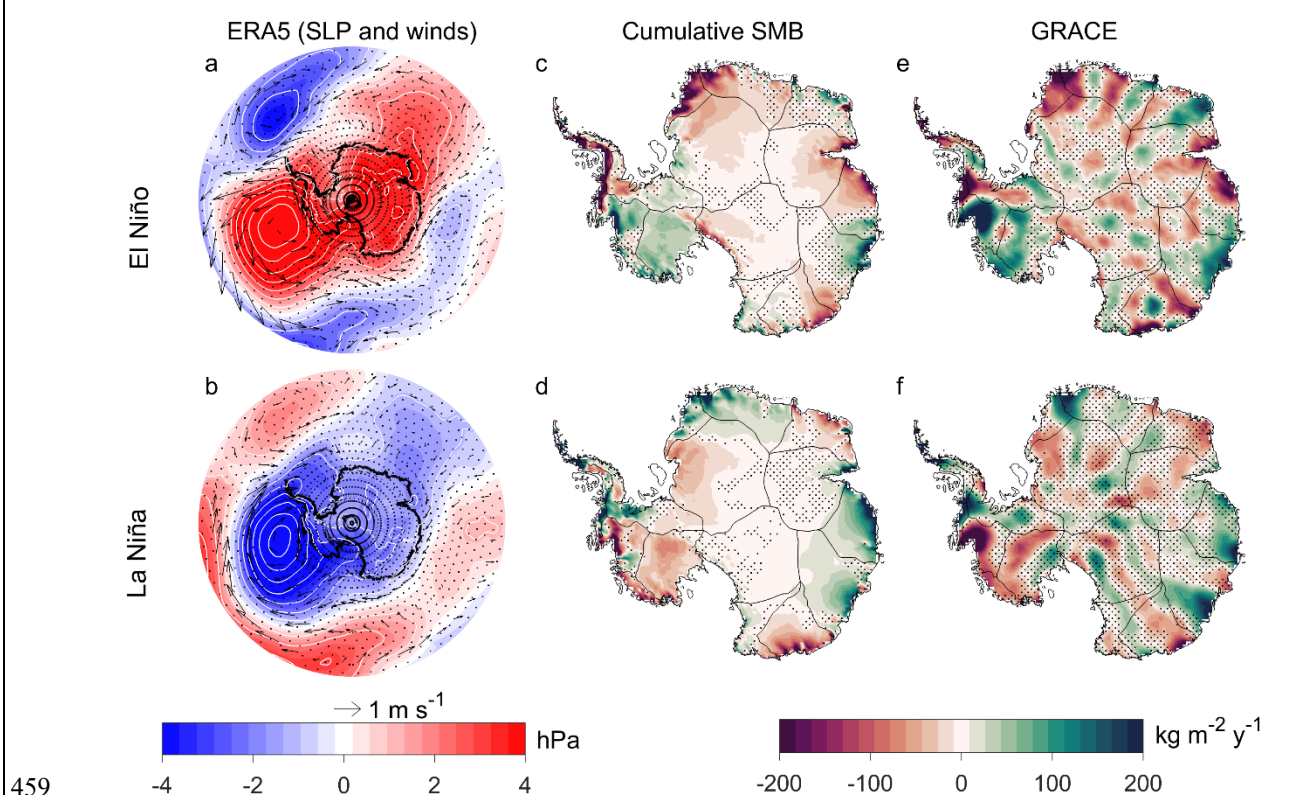
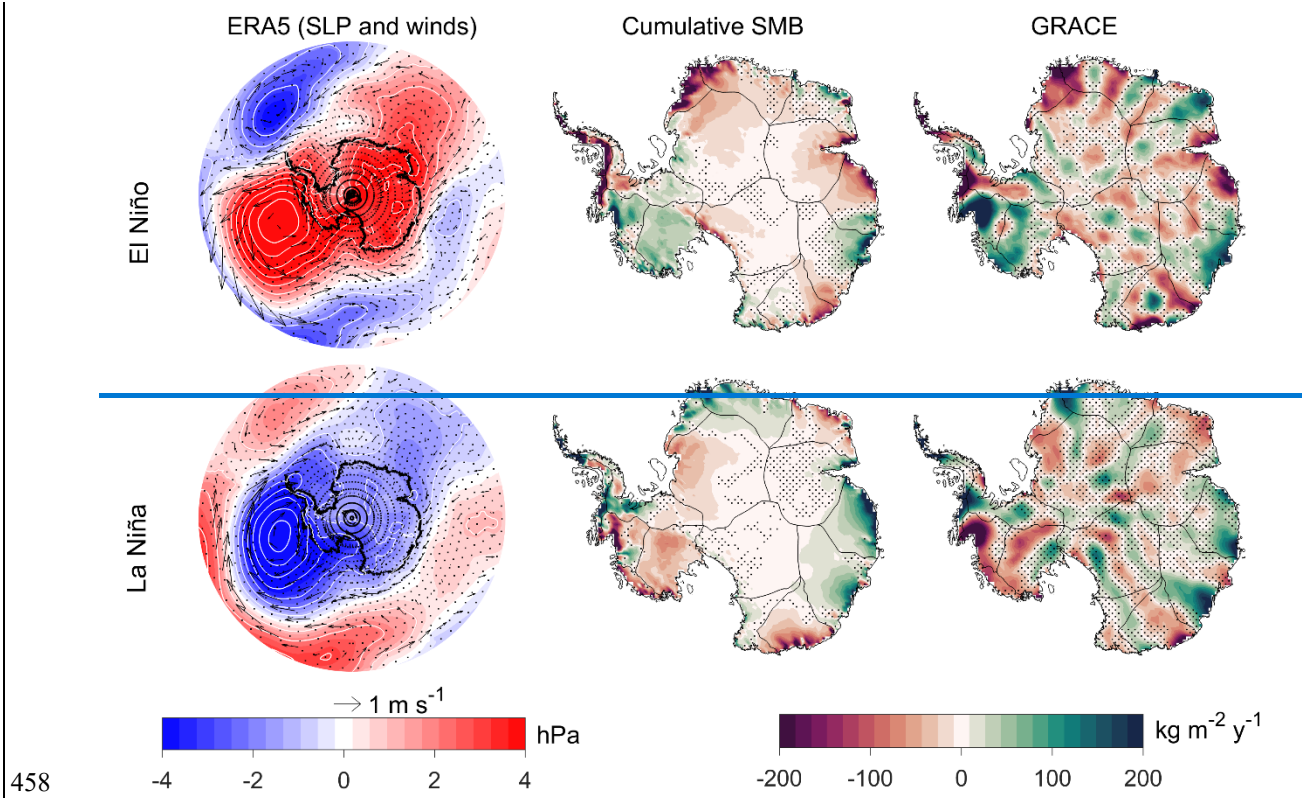
432 The negative pressure anomaly during the 2020–2022 La Niña period aligns with the observed mass gain in
433 Dronning Maud Land. Conversely, during the 2016–2018 period, negative SMB anomalies were observed in
434 Dronning Maud Land, with no clear pressure anomaly pattern (Fig. 5g).

435 In the Indian Ocean sector/Wilkes Land we found no consistent mass response to La Niña-dominated periods.
436 During the 2020–2022 La Niña period, mass change in the Indian Ocean sector is spatially uniform, with positive
437 mass anomalies observed across the entire region (Fig. 4h, l). This contrasts with other La Niña periods, which
438 show more variable responses. The 2010–2014 and 2016–2018 La Niña periods are consistent with each other,
439 showing negative mass anomalies over Wilkes Land. For both periods, a negative pressure anomaly is present
440 adjacent to the Wilkes Land coast, with the 2016–2018 period showing a statistically significant anomaly and
441 stronger negative mass signals. In contrast, the 2007–2009 and 2020–2022 La Niña periods are associated with
442 positive mass anomalies in Wilkes Land (Fig. 5i, l), although the anomalies during 2007–2009 are weaker and
443 less spatially extensive (Fig. 5i). During the 2007–2009 La Niña period, a positive pressure anomaly marginally
444 significant at the centre of the anomaly extends offshore along the Wilkes Land coast, associated with onshore
445 wind anomalies (Fig. 5a).

446 **3.4. Mean Anomalies during ENSO-dominated periods**

447 Figure 6 presents the mean AIS response across El Niño- and La Niña-dominated periods, summarizing the
448 impacts of different ENSO periods. The figure is derived by averaging the maps presented in Figures 4 and 5.
449 While this mean response differs slightly from the regression results in Fig. 3b–c, certain regional patterns remain
450 consistent. The SMB results show a positive response during El Niño-dominated periods in the Amundsen Sea
451 sector and Marie Byrd Land, as well as in Enderby Land (Fig. 6c). In contrast, negative SMB anomalies are
452 observed in the Antarctic Peninsula, Coats Land, and Dronning Maud Land (Fig. 6c). During La Niña-dominated
453 periods, this pattern is broadly reversed (Fig. 6d). Wilkes Land shows positive SMB anomalies during both El
454 Niño- and La Niña-dominated periods; however, the anomalies are more spatially extensive during La Niña (Fig.
455 6c–d). The patterns in GRACE are broadly similar to the SMB results, however, north south stripping noise in
456 GRACE is maximised over short periods.

457



460 **Figure 6.** The composites are generated based on the results of the four defined ENSO-dominated periods
 461 combined. ERA5 mean sea level pressure and 10 m wind anomalies (a–b), RACMO2.4p1 SMB (c–
 462 d), and GRACE-derived ice mass change (e–f). This represents the cumulative impact of
 463 different ENSO phases on AIS mass variability. Sea level pressure anomalies are shown as shaded regions

464 with contours (hPa), and 10 m wind anomalies [are indicated as](#) vectors (m s^{-1}). SMB and GRACE [data](#)
465 ($\text{kg m}^{-2} \text{y}^{-1}$) are shown. Non-significant areas [are](#) stippled at $p\text{-value} > 0.05$.

466 4. Discussion

467 4.1 Continental-wide perspective

468 We examined the AIS mass variability during different ENSO-dominated periods. Our results show that the AIS
469 exhibits considerable variability across these periods, each associated with its own circulation anomalies (Figs. 4,
470 5), influenced by interactions between ENSO and SAM (Hosking et al., 2013; Fogt et al., 2011). Over longer
471 timescales, the mean response reveals a dipole pattern: positive mass anomalies in West Antarctica and negative
472 anomalies in East Antarctic during El Niño periods, [with the reverse and vice-versa](#) during La Niña periods (Fig.
473 3b–c). This pattern is supported by data-driven analysis showing a strong correlation between GRACE and
474 cumulative ENSO indices (King et al., 2023).

475 However, there is a difference between the SMB signal and GRACE in West Antarctica, but they are closely
476 aligned in East Antarctica (Fig. 3b–c). This suggests that SMB variability drives [of](#) ice mass changes in East
477 Antarctica, but not necessarily in West Antarctica. The difference may be due to the near-instantaneous response
478 of ice dynamics to ENSO-driven oceanic forcing and/or mismodelled SMB (IMBIE Team, 2018; Rignot et al.,
479 2019), with the latter being more likely (King and Christoffersen, 2024).

480 Averaging multiple ENSO-dominated periods can obscure variability associated with individual periods and lead
481 to misinterpretation. As shown in Figs. 4e–h and 5e–h, mass variability—particularly in the Antarctic Peninsula
482 and East Antarctica—varies significantly across individual ENSO events (Figs. 4, 5). The mean response fails to
483 capture these short-term variations, which are critical for understanding their influence on AIS mass balance.

484 4.2 West Antarctica

485 El Niño-and La Niña-dominated periods correspond to positive and negative pressure anomalies in the Pacific,
486 respectively, indicative of positive PSA-1 and negative PSA-1 patterns (Hoskins and Karoly, 1981). These
487 patterns are associated with a weakened or strengthened ASL, influencing circulation and climate in West
488 Antarctica (Raphael et al., 2016b; Turner et al., 2017; Turner et al., 2012). Positive ice mass anomalies in the
489 Amundsen Sea sector during the 2002–2005, 2014–2016 and 2018–2020 El Niño periods (Fig. 4i, k–l) and
490 negative anomalies during the 2010–2014 and 2020–2022 La Niña periods (excluding the 2016–2018 period due
491 to noisy GRACE data) (Fig. 5i, k–l), are broadly consistent with previous studies (Paolo et al., 2018; King et al.,
492 2023). These mass anomalies are supported by the variability in the ASL during El Niño and La Niña periods
493 influencing circulation into the Amundsen Sea sector.

494 During El Niño conditions, a weakened ASL and reduced coastal easterlies allow westerly wind anomalies to
495 bring marine air masses, onshore, which, enhance snowfall and mass accumulation through orographic lifting
496 (Paolo et al., 2018; Huguenin et al., 2024). In contrast, La Niña conditions strengthen the ASL and intensify

497 coastal easterlies, limiting moisture transport and reducing precipitation (Huguenin et al., 2024; Hosking et al.,
498 2013).

499 However, the 2009–2010 El Niño period deviates from this pattern, with negative SMB anomalies observed in
500 the Amundsen Sea sector (Fig. 4f). The pressure anomaly during this period is distinct, with a positive pressure
501 anomaly extending from the Amundsen Sea to beyond the Ross Sea. An important difference to the other El Niño
502 periods, is the extension of this positive pressure anomaly further to the west, which decreases moisture transport
503 into the region. This period encompasses a strong Central Pacific El Niño event (Kim et al., 2011), and associated
504 pressure anomaly (Fig. 4b) resembles patterns linked to such events, which are associated with moisture depleted
505 wind anomalies and suppressed precipitation in the Amundsen and Bellingshausen regions (Chen et al., 2023;
506 Macha et al., 2024).

507 Our 2009-2010 El Niño mass pattern aligns with Macha et al. (2024), who reported reduced accumulation during
508 Central Pacific El Niño events in the SON and JJA seasons. These similarities suggest that the observed mass
509 change may reflect the impact of Central Pacific El Niño phases during the SON and JJA seasons in the Amundsen
510 Sea sector.

511 It is important to state that our defined ENSO periods do not distinguish between El Niño types or seasonal phases
512 but instead capture the net mass change over the entire period, providing broader context for ice sheet mass
513 balance.

514 Similarly, the 2007–2009 La Niña period shows a mass pattern that contrasts with other La Niña periods, featuring
515 a positive mass anomaly in the Amundsen Sea sector (Fig. 5i). However, atmospheric circulation patterns during
516 this period do not statistically support the observed mass gain, suggesting that it may be linked to unrelated
517 weather events or other modes of climate variability.

518 Our results support that mass variability in the Antarctic Peninsula is variable and influenced by various factors
519 such as large-scale climate modes including SAM and ENSO (Clem et al., 2016; Clem and Fogt, 2013) and the
520 Peninsula's unique mountainous geography. A previous study demonstrated a reduction in mass during El Niño
521 and an increase during La Niña across the Peninsula (Sasgen et al., 2010). This is consistent with our results for
522 the 2018–2020 El Niño- and 2020–2022 La Niña-dominated periods (Figs. 4l, 5l). Meanwhile, other studies
523 suggest the opposite pattern, reporting an increase in mass during El Niño and a reduction during La Niña in the
524 Peninsula (Zhang et al., 2021), which aligns with our observed ice mass change during the 2002-2005 and 2014-
525 2016 El Niño periods (Fig. 4i, k) and 2010-2014 La Niña period (Fig. 5j). However, the variable impact appears
526 to be influenced by the position and orientation of the ASL and its effect on moisture transport into the Peninsula
527 (Raphael et al., 2016a). Further, moisture transport into the Peninsula is influenced by SAM-driven westerly winds
528 and ENSO-related meridional flow (Orr et al., 2008; Clem et al., 2016), which contributes to the complex mass
529 change patterns.

530 4.3 East Antarctica

531 El Niño and La Niña events have been linked to negative and positive cumulative mass anomalies, respectively
532 in the East Antarctic Ice Sheet (King et al., 2023; Li et al., 2022), consistent with our earlier findings (Fig. 3b-c).

533 Our 2014–2016, 2018–2020 El Niño periods (Fig. 4k–l) and 2010–2014, 2020–2022 La Niña periods (Fig. 4j, l)
534 broadly align with this pattern. However, this pattern is consistent for every ENSO period (e.g., Figs. 4j, 5i), and
535 in some periods regionally variable responses observed across the Atlantic and Indian Ocean sectors.

536 SMB anomalies in East Antarctica are primarily influenced by the strength and position of cyclonic and
537 anticyclonic anomalies over the continent and the Southern Ocean (Figs. 4a–d and 5a–d). These pressure
538 anomalies regulate atmospheric circulation, with meridional flow changes affecting heat and moisture distribution
539 across the region (Scarchilli et al., 2011; Wang et al., 2024; Udy et al., 2021). The SAM phase largely governs
540 these pressure patterns by modulating their positioning which further and highlights its role as the dominant
541 role of SAM as a climate driver of mass change climate driver in East Antarctica (Fogt et al., 2012; Fogt and
542 Marshall, 2020a; Marshall et al., 2013). For instance, 2014–2016 El Niño showed a spatial mass change pattern
543 that are is consistent with a positive SAM phase, with a reduction in precipitation (Marshall et al., 2017) and
544 observed negative mass anomaly (Fig. 4g).

545 The anomalous mass gain during the 2009–2010 El Niño period observed in Dronning Maud Land has been
546 attributed to atmospheric blocking, which produced large episodic snowfall events (Boening et al., 2012).
547 Similarly, a positive pressure anomaly in the Atlantic during the 2010–2014 La Niña period (although not
548 significant at $p < 0.05$ over the 4-year period) appears to support the mass gain in the Dronning Maud Land (Fig.
549 5j). Atmospheric blocking favours the occurrence of atmospheric rivers reaching the Antarctic coastline, often
550 associated with increased precipitation and temperature (Wille et al., 2021; Pohl et al., 2021). The weakening of
551 the westerlies during negative SAM conditions (Clem et al., 2016), allows for Rossby wave amplification and an
552 increased frequency of atmospheric blocking events in East Antarctica, particularly during winter, when the
553 relationship is strongest (Wang et al., 2024). It is important to note that climate modes of variability can create
554 conditions favourable for atmospheric river events in East Antarctica (Shields et al., 2022), especially in Wilkes
555 Land (Wang, 2023). However, in Dronning Maud Land, atmospheric rivers explain about 77 % of interannual
556 variability- (Baiman et al., 2023).

557 Our 2002–2005 and 2009–2010 El Niño periods, along with the 2007–2009 La Niña period, show a blocking
558 pattern around Wilkes Land, consistent with transient meridional blocking associated with increased precipitation
559 along the coastline (Udy et al., 2022; Udy et al., 2021). However, given the duration of our defined periods, this
560 transient blocking is likely smoothed out over longer timeframes, which may explain the stronger signal observed
561 during the shorter 2009–2010 El Niño period. The asymmetric shape of the positive pressure anomaly extension
562 off the Wilkes Land is much stronger in the 2009–2010 period, and is consistent with the development of
563 atmospheric blocking in the Tasman Sea region (Pook et al., 2006), which is associated with increased
564 precipitation in Wilkes Land (Pohl et al., 2021; Udy et al., 2022).

565 Our 2020–2022 La Niña period shows significant mass gain across the Indian Ocean and Wilkes Land region and
566 was the only period in our analysis combining period when La Niña with and positive SAM occurred together
567 (Fig. 1c). However, this period also included the March 2022 atmospheric river event, which delivered record-
568 breaking precipitation and heat to East Antarctica (Wille et al., 2024). While this event was not the only
569 atmospheric river to occur during the GRACE period, this four-day event likely had some influenced on the mass
570 anomaly patterns of the 2020–2022 La Niña period we define in this study. To determine the extent of the

571 influence of this event, we examined the 2020–2022 period by comparing the inclusion and exclusion of the March
572 2022 event ([Supplementary](#) Fig. S5). While the March 2022 event increased the strength of the SMB positive
573 anomaly in Wilkes Land, the region still observed a strong positive SMB anomaly during the 2020–2022 period
574 when March 2022 was excluded ([Supplementary](#) Fig. S5). According to Wang et al. (2023), extreme events in
575 [October 2021](#) and March 2022 [and October 2021](#) accounted for approximately 38% of the precipitation anomalies
576 in Wilkes Land during the 2020–2022 La Niña period, driven by a pair of symmetrically distributed high–low
577 pressure systems over the Southern Ocean near 120°W and 60°E.

578 Our findings indicate that ice mass changes during ENSO-dominated periods cannot be solely attributed to ENSO
579 forcing. To quantify changes in ENSO variability, long-[term](#) time series must be considered in future studies
580 (Stevenson et al., 2010), along with the use of climate models to better isolate and capture purely ENSO-driven
581 signals.

582 **4.4 Combined ENSO and SAM influence**

583 Isolating the ENSO signal and its impact on AIS ice mass is challenging due to several factors. The Rossby wave
584 propagation of the ENSO signal to Antarctica is influenced by SAM (Marshall, 2003; Fogt and Marshall, 2020b),
585 and the ENSO signal can be masked by other climate modes, such as zonal-wave 3—a quasi-stationary pattern in
586 the southern high latitudes that affects meridional heat and momentum transport (Goyal et al., 2022; Raphael,
587 2004). Additionally, synoptic-scale weather systems can further mask ENSO’s influence. The complex interaction
588 between ENSO and other modes of climate variability likely drives the equally complex patterns of AIS ice mass
589 change observed during different ENSO-dominated periods.

590 Pressure anomaly variability in the Pacific sector during ENSO-dominated periods can be associated with the
591 cumulative SAM phase. During ENSO periods when the cumulative SAM and ENSO occur in phase (El Niño/–
592 SAM or La Niña/+SAM) (Fogt et al., 2011), the pressure anomaly over the Pacific sector is close to the continent,
593 spatially extensive, and centred around the Amundsen Sea sector (Figs. 4a and 5d). However, during ENSO-
594 dominated periods that are out of phase with the cumulative SAM (El Niño/+SAM or La Niña/–SAM) (Fogt et
595 al., 2011), the pressure anomaly appears northward, away from the continent (Figs. 4c and 5a). Periods where the
596 cumulative SAM [indexphase](#) shows a neutral phase, the pressure anomaly in the Pacific is centred around the
597 Bellingshausen Sea sector (Figs. 4d, 5b–c). However, between 2000 [and](#) 2020, shifts in large-scale circulation,
598 particularly in SAM, have been reported, potentially affecting ENSO teleconnections and their influence on AIS
599 variability (Xin et al., 2023).

600 Our analysis, which uses cumulative summed indices to match GRACE mass time series, has limitations. It
601 focuses primarily on low-frequency variability and does not account for shorter temporal scale impacts, such as
602 tropical convection pulses that trigger the Rossby waves or high-frequency variability associated with storm
603 systems such as atmospheric rivers. However, the net effect of these would be captured by GRACE.

604 Studies on precipitation (Marshall et al., 2017) and ice core records (Medley and Thomas, 2019) both recognise
605 that SMB generally decreases during positive SAM phase and increases during negative SAM phase. [In-terms](#)
606 [of](#) [Regarding](#) the impact [of](#) [SAM](#) on basal melting, negative SAM periods generally decrease the transport of warm

607 circumpolar deep water onto the continental shelf (Palóczy et al., 2018), largely reducing ice shelf basal melt
608 (Verfaillie et al., 2022) and subsequently contributing to ice mass gain. However, the timescale of the upstream
609 ice response of the upstream ice to the positive SAM forcing is unclear and would involve a substantial lag, which
610 can range from months to several years depending on regional ice dynamics (King and Christoffersen, 2024). This
611 suggests that GRACE-derived signals may represent a delayed response rather than an immediate reaction to SAM
612 variability. The spatial pattern of ice mass change anomaly during the 2002–2005 El Niño and 2007–2009 La
613 Niña-dominated periods in the Amundsen Sea sector and Wilkes Land resembles the negative SAM spatial pattern
614 reported by King et al. (2023). Negative SAM dominates the cumulative summed SAM (Fig. 1e) from the start of
615 the GRACE time series in 2002 until around 2010, which aligns with the positive pressure anomaly observed over
616 Antarctica, reflecting a stronger than average (over the GRACE period) Antarctic High during this period (Figs.
617 4a–b and 5a). Therefore, it is possible that ice mass variability observed between 2002 and 2010 was more
618 influenced by SAM than by ENSO.

619 Our findings agree with the premise that ENSO forcing on the Antarctic climate impacts atmospheric circulation
620 patterns, altering the ASL variability, which in turn influences Antarctic ice mass variability (Zhang et al., 2021;
621 Paolo et al., 2018; Sasgen et al., 2010; Clem et al., 2017). However, across individual ENSO periods, the AIS
622 response exhibits considerable variability, with each period associated with distinct atmospheric circulation
623 patterns. It is possible that the teleconnection between tropical ENSO signals and Antarctic climate may not be
624 fully established during a given ENSO phase or masked by other processes. Our analysis, which uses cumulative
625 summed indices to match GRACE mass time series, is primarily sensitive to low-frequency variability and does
626 not resolve shorter-term impacts, such as tropical convection pulses that initiate Rossby wave trains or high-
627 frequency variability linked to storm systems like atmospheric rivers. Nonetheless, the integrated effect of these
628 processes is captured by GRACE. Additionally, internal dynamics of the ASL may contribute to AIS mass
629 variability that is independent of the influence of ENSO and SAM which potentially can impact our analysis.
630 Given that our analysis spans a 22-year period, it is insufficient to capture the full range of ENSO variability,
631 which requires a longer time period to be fully represented~~long time series must be considered in future studies~~
632 (Stevenson et al., 2010). Future studies should therefore consider a longer record, along~~together~~with the use of
633 climate models~~s~~ to better isolate and capture purely ENSO-driven signals. While ENSO induced circulation affects
634 Antarctic SMB (Kim et al., 2020), recent Antarctic ice mass trends (2003-2020) have been primarily driven by
635 mass imbalance triggered by long-term ice dynamics changes (Kim et al., 2024; Rignot et al., 2019). Some of the
636 low-frequency mass variability around the long-term trend (which we removed) is associated with changing ice
637 dynamics. This dynamic signal is stronger in West than in East Antarctica (Rignot et al., 2019).

638 In a warming climate, future ENSO event variability is predicted to increase (Cai et al., 2021). CMIP5 model
639 simulations suggest a reduction in El Niño-induced precipitation over West Antarctica (Lee et al., 2023). Given
640 that SAM is projected to remain in its positive phase across all seasons due to greenhouse gas emissions (Arblaster
641 and Meehl, 2006), accurate modelling of future AIS mass estimates in relation to ENSO teleconnections must
642 account for the interaction between SAM and ENSO. The AIS mass gain observed during 2020–2022 raises
643 questions about how the AIS will respond to future La Niña and positive SAM periods and if it would increase
644 the frequency of extreme events.

645 **5 Conclusion**

646 To examine the AIS mass change during different ENSO-dominated periods, we analysed AIS mass change
647 anomalies observed by GRACE/GRACE-FO spanning the period 2002-2022. These anomalies were interpreted
648 alongside RACMO2.4p1 modelled SMB and mean sea level pressure and 10 m winds from ERA5 reanalysis
649 products. Our analysis reveals that El Niño and La Niña periods exert distinct influences on the AIS, with
650 considerable spatial variability.

651 At the continental scale, three out of the four El Niño-dominated periods were characterised by mass increase in
652 West Antarctica and mass decrease in East Antarctica. Conversely, two out of the three La Niña-dominated
653 periods (here excluding the 2016-2018 period with degraded GRACE signal) showed the opposite pattern, with
654 mass reduction in West Antarctica and to varying degrees, mass increase in East Antarctica. The Amundsen Sea
655 sector typically experiences positive mass anomalies during El Niño-dominated periods and negative anomalies
656 during La Niña-dominated periods.

657 Mass variability in West Antarctica is primarily driven by ENSO-induced ASL pressure anomalies, which
658 modulate the atmospheric circulation and moisture transport. The ASL exhibits high variability in its location,
659 strength, and extent, which influences its impact onbetween the Antarctic Peninsula and West Antarctica. The
660 ASL strengthens and moves closer to the Antarctic coastline during periods when ENSO-SAM are in phase
661 (Hosking et al., 2013). While ENSO has its strongest impact in West Antarctica. In East Antarctica However,
662 atmospheric pressure patterns over the Southern Ocean play a crucial role in regulating moisture influx and,
663 consequently, ice mass variability in East Antarctica affecting ice mass variability.

664 In summary, this study highlights the complex nature of ENSO teleconnections in modulating AIS mass balance
665 through changes in atmospheric circulation. Rather than exhibiting a simple dipole response, AIS mass variability
666 during ENSO periods is shaped by unique teleconnections and moisture fluxes specific to each period. We
667 acknowledge uncertainties in our analysis due to the relatively short ENSO-dominated periods considered. Some
668 ENSO-related teleconnections may not have fully developed during these intervals, and other processes—such as
669 atmospheric rivers—may have masked or modulated the ENSO signal, complicating the attribution of the
670 observed spatial impacts. Although climate model projections remain uncertain regarding whether future ENSO
671 events will more resemble more an El Niño- or La Niña-like state, they consistently indicate that ENSO will
672 influence Antarctic precipitation patterns. A clearer understanding of ENSO's role in Antarctic climate is therefore
673 critical for assessing its impact on future SMB and long-term ice mass balance. This requires both process-level
674 understanding and consideration of the net ENSO effect on ice sheet AIS mass change as explored here.

675 **Code and Data availability**

676 Source code and data will be made available through the University of Tasmania Research Data Portal prior to
677 publication. The GRACE data used is available at <https://gravis.gfz.de/ais>. The ERA5 reanalysis data used in the
678 atmospheric linkage to ice mass variation are publicly available from <https://cds.climate.copernicus.eu/>. The
679 station-derived SAM index from Marshall (2003) [are](#) available at <http://www.nerc-bas.ac.uk/icd/gjma/sam.html>.
680 The Niño3.4 index are publicly available from <https://psl.noaa.gov/data/timeseries/month/Nino34/>.
681 RACMO2.4p1 model SMB output can be accessed at <https://zenodo.org/records/14217232> (Van Dalum et al.,
682 2025; Van Dalum et al., 2024).

683 **Author contributions**

684 All authors contributed to the conception and design of the study. JBA performed the statistical analysis and data
685 processing. JBA wrote the manuscript with input from all co-authors. All authors helped with the revision and
686 approved the final version of the manuscript.

687 **Competing interests**

688 The authors declare that they have no conflict of interest.

689 **Disclaimer**

690 Publisher's note: Copernicus Publications remains neutral with regard to jurisdictional claims made in the text,
691 published maps, institutional affiliations, or any other geographical representation in this paper. While Copernicus
692 Publications makes every effort to include appropriate place names, the final responsibility lies with the authors.

693 **Acknowledgements**

694 We thank the GravIS team for supplying GRACE data, the European Centre for Medium-Range Weather
695 Forecasts for providing reanalysis climatic data, NOAA for the ENSO indices, Marshall (2003) for the SAM index
696 and Van Dalum et al. (2024) [for providing the RACMO2.4p1 SMB dataset](#). Finally, we thank the Editor and
697 reviewers for constructive reviews.

698 **Financial support**

699 JBA, MK and DU were supported by the Australian Research Council Special Research Initiative, Australian
700 Centre for Excellence in Antarctic Science (Project Number SR200100008). TV was supported by the Australian
701 Government's Antarctic Science Collaboration Initiative (ASCI000002) through funding to the Australian
702 Antarctic Program Partnership. JBA was supported by a University of Tasmania Graduate Research Scholarship.

703 **References**

704 [Arblaster, J. M. and Meehl, G. A.: Contributions of external forcings to southern annular mode trends, Journal of](#)
705 [Climate, 19, 2896-2905, Doi 10.1175/Jcli3774.1, 2006.](#)
706 [Baiman, R., Winters, A. C., Lenaerts, J., and Shields, C. A.: Synoptic Drivers of Atmospheric River Induced](#)
707 [Precipitation Near Dronning Maud Land, Antarctica, Journal of Geophysical Research \(Atmospheres\), 128,](#)
708 [e2022JD037859, 10.1029/2022jd037859, 2023.](#)

709 [Bodart, J. A. and Bingham, R. J.: The Impact of the Extreme 2015-2016 El Nino on the Mass Balance of the](#)
710 [Antarctic Ice Sheet, Geophysical Research Letters, 46, 13862-13871, 10.1029/2019gl084466, 2019.](#)

711 [Boening, C., Lebsock, M., Landerer, F., and Stephens, G.: Snowfall-driven mass change on the East Antarctic ice](#)
712 [sheet, Geophysical Research Letters, 39, n/a-n/a, Artn L21501](#)
713 [10.1029/2012gl053316, 2012.](#)

714 [Cai, W. J., Santoso, A., Collins, M., Dewitte, B., Karamperidou, C., Kug, J. S., Lengaigne, M., McPhaden, M. J.,](#)
715 [Stuecker, M. F., Taschetto, A. S., Timmermann, A., Wu, L. X., Yeh, S. W., Wang, G. J., Ng, B., Jia, F., Yang,](#)
716 [Y., Ying, J., Zheng, X. T., Bayr, T., Brown, J. R., Capotondi, A., Cobb, K. M., Gan, B. L., Geng, T., Ham, Y. G.,](#)
717 [Jin, F. F., Jo, H. S., Li, X. C., Lin, X. P., McGregor, S., Park, J. H., Stein, K., Yang, K., Zhang, L., and Zhong,](#)
718 [W. X.: Changing El Nino-Southern Oscillation in a warming climate, Nature Reviews Earth & Environment, 2,](#)
719 [628-644, 10.1038/s43017-021-00199-z, 2021.](#)

720 [Chen, X. Y., Li, S. L., and Zhang, C.: Distinct impacts of two kinds of El Nino on precipitation over the Antarctic](#)
721 [Peninsula and West Antarctica in austral spring, Atmospheric and Oceanic Science Letters, 16, 100387, ARTN](#)
722 [100387](#)
723 [10.1016/j.aosl.2023.100387, 2023.](#)

724 [Clem, K. R. and Fogt, R. L.: Varying roles of ENSO and SAM on the Antarctic Peninsula climate in austral spring,](#)
725 [J Geophys Res-Atmos, 118, 11481-11492, 10.1002/jgrd.50860, 2013.](#)

726 [Clem, K. R., Renwick, J. A., and McGregor, J.: Large-Scale Forcing of the Amundsen Sea Low and Its Influence](#)
727 [on Sea Ice and West Antarctic Temperature, Journal of Climate, 30, 8405-8424, 10.1175/Jcli-D-16-0891.1, 2017.](#)

728 [Clem, K. R., Renwick, J. A., McGregor, J., and Fogt, R. L.: The relative influence of ENSO and SAM on Antarctic](#)
729 [Peninsula climate, J Geophys Res-Atmos, 121, 9324-9341, 10.1002/2016jd025305, 2016.](#)

730 [Dahle, C., Murböck, M., Flechtnner, F., Dobslaw, H., Michalak, G., Neumayer, K. H., Abrykosov, O., Reinhold,](#)
731 [A., König, R., Sulzbach, R., and Förste, C.: The GFZ GRACE RL06 Monthly Gravity Field Time Series:](#)
732 [Processing Details and Quality Assessment, Remote Sensing, 11, 2116, ARTN 2116](#)
733 [10.3390/rs11182116, 2019.](#)

734 [Dahle, C., Boergens, E., Sasgen, I., Döhne, T., Reißland, S., Dobslaw, H., Kleemann, V., Murböck, M., König, R.,](#)
735 [Dill, R., Sips, M., Sylla, U., Groh, A., Horwath, M., and Flechtnner, F.: GravIS: mass anomaly products from](#)
736 [satellite gravimetry, 10.5194/essd-2024-347, 2024.](#)

737 [Diener, T., Sasgen, I., Agosta, C., Fuerst, J. J., Braun, M. H., Konrad, H., and Fettweis, X.: Acceleration of](#)
738 [Dynamic Ice Loss in Antarctica From Satellite Gravimetry, Frontiers in Earth Science, 9, ARTN 741789](#)
739 [10.3389/feart.2021.741789, 2021.](#)

740 [Fogt, R. L. and Marshall, G. J.: The Southern Annular Mode: Variability, trends, and climate impacts across the](#)
741 [Southern Hemisphere, WIREs Climate Change, 11, 10.1002/wcc.652, 2020a.](#)

742 [Fogt, R. L. and Marshall, G. J.: The Southern Annular Mode: Variability, trends, and climate impacts across the](#)
743 [Southern Hemisphere, Wiley Interdisciplinary Reviews-Climate Change, 11, ARTN e652](#)
744 [10.1002/wcc.652, 2020b.](#)

745 [Fogt, R. L., Bromwich, D. H., and Hines, K. M.: Understanding the SAM influence on the South Pacific ENSO](#)
746 [teleconnection, Climate Dyn., 36, 1555-1576, 2011.](#)

747 [Fogt, R. L., Jones, J. M., and Renwick, J.: Seasonal Zonal Asymmetries in the Southern Annular Mode and Their](#)
748 [Impact on Regional Temperature Anomalies, Journal of Climate, 25, 6253-6270, 10.1175/jcli-d-11-00474.1,](#)
749 [2012.](#)

750 [Gardner, A. S., Moholdt, G., Scambos, T., Fahnestock, M., Ligtenberg, S., van den Broeke, M., and Nilsson, J.:](#)
751 [Increased West Antarctic and unchanged East Antarctic ice discharge over the last 7 years, Cryosphere, 12, 521-](#)
752 [547, 10.5194/tc-12-521-2018, 2018.](#)

753 [Goyal, R., Jucker, M., Gupta, A. S., and England, M. H.: A New Zonal Wave-3 Index for the Southern](#)
754 [Hemisphere, Journal of Climate, 35, 5137-5149, 10.1175/Jcli-D-21-0927.1, 2022.](#)

755 [Groh, A. and Horwath, M.: The method of tailored sensitivity kernels for GRACE mass change estimates, April](#)
756 [01, 20162016.](#)

757 [Hersbach, H., Bell, B., Berrisford, P., Hirahara, S., Horányi, A., Muñoz-Sabater, J., Nicolas, J., Peubey, C., Radu,](#)
758 [R., Schepers, D., Simmons, A., Soci, C., Abdalla, S., Abellán, X., Balsamo, G., Bechtold, P., Biavati, G., Bidlot,](#)
759 [J., Bonavita, M., De Chiara, G., Dahlgren, P., Dee, D., Diamantakis, M., Dragani, R., Flemming, J., Forbes, R.,](#)
760 [Fuentes, M., Geer, A., Haimberger, L., Healy, S., Hogan, R. J., Hólm, E., Janisková, M., Keeley, S., Laloyaux,](#)
761 [P., Lopez, P., Lupu, C., Radnoti, G., de Rosnay, P., Rozum, I., Vamborg, F., Villaume, S., and Thépaut, J. N.:](#)
762 [The ERA5 global reanalysis, Quarterly Journal of the Royal Meteorological Society, 146, 1999-2049,](#)
763 [10.1002/qj.3803, 2020.](#)

764 [Hosking, J. S., Orr, A., Marshall, G. J., Turner, J., and Phillips, T.: The Influence of the Amundsen-Bellingshausen](#)
765 [Seas Low on the Climate of West Antarctica and Its Representation in Coupled Climate Model Simulations,](#)
766 [Journal of Climate, 26, 6633-6648, 10.1175/Jcli-D-12-00813.1, 2013.](#)

767 [Hoskins, B. J. and Karoly, D. J.: The Steady Linear Response of a Spherical Atmosphere to Thermal and](#)
768 [Orographic Forcing, Journal of the Atmospheric Sciences, 38, 1179-1196, Doi 10.1175/1520-0469\(1981\)038<1179:Tslroa>2.0.Co;2, 1981.](#)

770 [Huguenin, M. F., Holmes, R. M., Spence, P., and England, M. H.: Subsurface Warming of the West Antarctic](#)
771 [Continental Shelf Linked to El Niño-Southern Oscillation, Geophysical Research Letters, 51, ARTN](#)
772 [e2023GL104518](#)
773 [10.1029/2023GL104518, 2024.](#)

774 [Kim, B. H., Seo, K. W., Eom, J., Chen, J., and Wilson, C. R.: Antarctic ice mass variations from 1979 to 2017](#)
775 [driven by anomalous precipitation accumulation, Sci Rep, 10, 20366, 10.1038/s41598-020-77403-5, 2020.](#)

776 [Kim, B. H., Seo, K. W., Lee, C. K., Kim, J. S., Lee, W. S., Jin, E. K., and van den Broeke, M.: Partitioning the](#)
777 [drivers of Antarctic glacier mass balance \(2003-2020\) using satellite observations and a regional climate model,](#)
778 [Proc Natl Acad Sci U S A, 121, e2322622121, 10.1073/pnas.2322622121, 2024.](#)

779 [King, M. A. and Christoffersen, P.: Major Modes of Climate Variability Dominate Nonlinear Antarctic Ice-Sheet](#)
780 [Elevation Changes 2002-2020, Geophysical Research Letters, 51, ARTN e2024GL108844](#)
781 [10.1029/2024GL108844, 2024.](#)

782 [King, M. A., Lyu, K., and Zhang, X. B.: Climate variability a key driver of recent Antarctic ice-mass change,](#)
783 [Nature Geoscience, 16, 1128-1135, 10.1038/s41561-023-01317-w, 2023.](#)

784 [Landerer, F. W., Flechtner, F. M., Save, H., Webb, F. H., Bandikova, T., Bertiger, W. I., Bettadpur, S. V., Byun,](#)
785 [S. H., Dahle, C., Dobslaw, H., Fahnestock, E., Harvey, N., Kang, Z. G., Kruizinga, G. L. H., Loomis, B. D.,](#)
786 [McCullough, C., Murböck, M., Nagel, P., Paik, M., Pie, N., Poole, S., Strekalov, D., Tamisiea, M. E., Wang, F.](#)
787 [R., Watkins, M. M., Wen, H. Y., Wiese, D. N., and Yuan, D. N.: Extending the Global Mass Change Data Record:](#)
788 [GRACE Follow-On Instrument and Science Data Performance, Geophysical Research Letters, 47, ARTN](#)
789 [e2020GL088306](#)
790 [10.1029/2020GL088306, 2020.](#)

791 [Lee, H.-J., Jin, E. K., Kim, B.-H., and Lee, W. S.: Vanishing of the El Niño-induced delay effect on the ice mass](#)
792 [loss of West Antarctica in future climate change, 10.21203/rs.3.rs-2437498/v1, 2023.](#)

793 [Li, Z., Chao, B. F., Wang, H., and Zhang, Z.: Antarctica ice-mass variations on interannual timescale: Coastal](#)
794 [Dipole and propagating transports, Earth and Planetary Science Letters, 595, 117789, ARTN 117789](#)
795 [10.1016/j.epsl.2022.117789, 2022.](#)

796 [Macha, J. M. A., Mackintosh, A. N., McCormack, F. S., Henley, B. J., McGregor, H. V., van Dalum, C. T., and](#)
797 [Purich, A.: Distinct Central and Eastern Pacific El Niño Influence on Antarctic Surface Mass Balance,](#)
798 [Geophysical Research Letters, 51, ARTN e2024GL109423](#)
799 [10.1029/2024GL109423, 2024.](#)

800 [Marshall, G. J.: Trends in the southern annular mode from observations and reanalyses, Journal of Climate, 16,](#)
801 [4134-4143, Doi 10.1175/1520-0442\(2003\)016<4134:Titam>2.0.Co;2, 2003.](#)

802 [Marshall, G. J., Orr, A., and Turner, J.: A Predominant Reversal in the Relationship between the SAM and East](#)
803 [Antarctic Temperatures during the Twenty-First Century, Journal of Climate, 26, 5196-5204, 10.1175/Jcli-D-12-](#)
804 [00671.1, 2013.](#)

805 [Marshall, G. J., Thompson, D. W. J., and van den Broeke, M. R.: The Signature of Southern Hemisphere](#)
806 [Atmospheric Circulation Patterns in Antarctic Precipitation, Geophys Res Lett, 44, 11580-11589,](#)
807 [10.1002/2017GL075998, 2017.](#)

808 [McPhaden, M. J., Zebiak, S. E., and Glantz, M. H.: ENSO as an integrating concept in earth science, Science,](#)
809 [314, 1740-1745, 10.1126/science.1132588, 2006.](#)

810 [Medley, B. and Thomas, E. R.: Increased snowfall over the Antarctic Ice Sheet mitigated twentieth-century sea-](#)
811 [level rise, Nature Climate Change, 9, 34+, 10.1038/s41558-018-0356-x, 2019.](#)

812 [Orr, A., Marshall, G. J., Hunt, J. C. R., Sommeria, J., Wang, C.-G., Van Lipzig, N. P. M., Cresswell, D., and King,](#)
813 [J. C.: Characteristics of Summer Airflow over the Antarctic Peninsula in Response to Recent Strengthening of](#)
814 [Westerly Circumpolar Winds, Journal of the Atmospheric Sciences, 65, 1396-1413, 10.1175/2007jas2498.1,](#)
815 [2008.](#)

816 [Palócz, A., Gille, S. T., and McClean, J. L.: Oceanic Heat Delivery to the Antarctic Continental Shelf: Large-](#)
817 [Scale, Low-Frequency Variability, Journal of Geophysical Research: Oceans, 123, 7678-7701,](#)
818 [10.1029/2018jc014345, 2018.](#)

819 [Paolo, F. S., Padman, L., Fricker, H. A., Adusumilli, S., Howard, S., and Siegfried, M. R.: Response of Pacific-](#)
820 [sector Antarctic ice shelves to the El Niño/Southern Oscillation, Nat Geosci, 11, 121-126, 10.1038/s41561-017-](#)
821 [0033-0, 2018.](#)

822 [Pohl, B., Favier, V., Wille, J., Udy, D. G., Vance, T. R., Pergaud, J., Dutrievoz, N., Blanchet, J., Kittel, C., Amory,](#)
823 [C., Krinner, G., and Codron, F.: Relationship Between Weather Regimes and Atmospheric Rivers in East](#)
824 [Antarctica, Journal of Geophysical Research: Atmospheres, 126, 10.1029/2021jd035294, 2021.](#)

825 Pook, M. J., McIntosh, P. C., and Meyers, G. A.: The Synoptic Decomposition of Cool-Season Rainfall in the
826 Southeastern Australian Cropping Region, *Journal of Applied Meteorology and Climatology*, 45, 1156-1170,
827 10.1175/jam2394.1, 2006.

828 Raphael, M. N.: A zonal wave 3 index for the Southern Hemisphere, *Geophysical Research Letters*, 31, n/a-n/a,
829 Artn L23212
830 10.1029/2004gl020365, 2004.

831 Raphael, M. N., Marshall, G. J., Turner, J., Fogt, R. L., Schneider, D., Dixon, D. A., Hosking, J. S., Jones, J. M.,
832 and Hobbs, W. R.: The Amundsen Sea Low: Variability, Change, and Impact on Antarctic Climate, *Bulletin of
833 the American Meteorological Society*, 97, 111-121, 10.1175/bams-d-14-00018.1, 2016a.

834 Raphael, M. N., Marshall, G. J., Turner, J., Fogt, R. L., Schneider, D., Dixon, D. A., Hosking, J. S., Jones, J. M.,
835 and Hobbs, W. R.: THE AMUNDSEN SEA LOW Variability, Change, and Impact on Antarctic Climate, *Bulletin
836 of the American Meteorological Society*, 97, 111-121, 10.1175/Bams-D-14-00018.1, 2016b.

837 Rayner, N. A., Parker, D. E., Horton, E. B., Folland, C. K., Alexander, L. V., Rowell, D. P., Kent, E. C., and
838 Kaplan, A.: Global analyses of sea surface temperature, sea ice, and night marine air temperature since the late
839 nineteenth century, *J Geophys Res-Atmos*, 108, Artn 4407
840 10.1029/2002jd002670, 2003.

841 Richard Peltier, W., Argus, D. F., and Drummond, R.: Comment on “An Assessment of the ICE-6G C (VM5a)
842 Glacial Isostatic Adjustment Model” by Purcell et al, *Journal of Geophysical Research: Solid Earth*, 123, 2019-
843 2028, 10.1002/2016jb013844, 2018.

844 Rignot, E., Mouginot, J., Scheuchl, B., van den Broeke, M., van Wessem, M. J., and Morlighem, M.: Four decades
845 of Antarctic Ice Sheet mass balance from 1979-2017, *Proc Natl Acad Sci U S A*, 116, 1095-1103,
846 10.1073/pnas.1812883116, 2019.

847 Sasgen, I., Groh, A., and Horwath, M.: COST-G GravIS RL01 ice-mass change products, 2020.

848 Sasgen, I., Dobslaw, H., Martinec, Z., and Thomas, M.: Satellite gravimetry observation of Antarctic snow
849 accumulation related to ENSO, *Earth and Planetary Science Letters*, 299, 352-358, 10.1016/j.epsl.2010.09.015,
850 2010.

851 Scarchilli, C., Frezzotti, M., and Ruti, P. M.: Snow precipitation at four ice core sites in East Antarctica:
852 provenance, seasonality and blocking factors, *Climate Dynamics*, 37, 2107-2125, 10.1007/s00382-010-0946-4,
853 2011.

854 Schneider, D. P., Okumura, Y., and Deser, C.: Observed Antarctic Interannual Climate Variability and Tropical
855 Linkages, *Journal of Climate*, 25, 4048-4066, 10.1175/Jcli-D-11-00273.1, 2012.

856 Shepherd, A., Ivins, E. R., A. G., Barletta, V. R., Bentley, M. J., Bettadpur, S., Briggs, K. H., Bromwich, D. H.,
857 Forsberg, R., Galin, N., Horwath, M., Jacobs, S., Joughin, I., King, M. A., Lenaerts, J. T., Li, J., Ligtenberg, S.
858 R., Luckman, A., Luthcke, S. B., McMillan, M., Meister, R., Milne, G., Mouginot, J., Muir, A., Nicolas, J. P.,
859 Paden, J., Payne, A. J., Pritchard, H., Rignot, E., Rott, H., Sorenson, L. S., Scambos, T. A., Scheuchl, B., Schrama,
860 E. J., Smith, B., Sundal, A. V., van Angelen, J. H., van de Berg, W. J., van den Broeke, M. R., Vaughan, D. G.,
861 Velicogna, I., Wahr, J., Whitehouse, P. L., Wingham, D. J., Yi, D., Young, D., and Zwally, H. J.: A reconciled
862 estimate of ice-sheet mass balance, *Science*, 338, 1183-1189, 10.1126/science.1228102, 2012.

863 Shields, C. A., Wille, J. D., Marquardt Collow, A. B., MacLennan, M., and Gorodetskaya, I. V.: Evaluating
864 Uncertainty and Modes of Variability for Antarctic Atmospheric Rivers, *Geophysical Research Letters*, 49,
865 10.1029/2022gl099577, 2022.

866 Stevenson, S., Fox-Kemper, B., Jochum, M., Rajagopalan, B., and Yeager, S. G.: ENSO Model Validation Using
867 Wavelet Probability Analysis, *Journal of Climate*, 23, 5540-5547, 10.1175/2010jcli3609.1, 2010.

868 Swenson, S., Chambers, D., and Wahr, J.: Estimating geocenter variations from a combination of GRACE and
869 ocean model output, *Journal of Geophysical Research-Solid Earth*, 113, Artn B08410
870 10.1029/2007jb005338, 2008.

871 Tapley, B. D., Bettadpur, S., Ries, J. C., Thompson, P. F., and Watkins, M. M.: GRACE measurements of mass
872 variability in the Earth system, *Science*, 305, 503-505, 10.1126/science.1099192, 2004.

873 team, I.: Mass balance of the Antarctic Ice Sheet from 1992 to 2017, *Nature*, 558, 219-222, 10.1038/s41586-018-
874 0179-y, 2018.

875 Turner, J.: The El Nino-southern oscillation and Antarctica, *International Journal of Climatology*, 24, 1-31,
876 10.1002/joc.965, 2004.

877 Turner, J., Phillips, T., Hosking, J. S., Marshall, G. J., and Orr, A.: The Amundsen Sea low, *International Journal
878 of Climatology*, 33, 1818-1829, 10.1002/joc.3558, 2012.

879 Turner, J., Orr, A., Gudmundsson, G. H., Jenkins, A., Bingham, R. G., Hillenbrand, C. D., and Bracegirdle, T. J.:
880 Atmosphere-ocean-ice interactions in the Amundsen Sea Embayment, West Antarctica, *Reviews of Geophysics*,
881 55, 235-276, 10.1002/2016rg000532, 2017.

882 Udy, D. G., Vance, T. R., Kiem, A. S., and Holbrook, N. J.: A synoptic bridge linking sea salt aerosol
883 concentrations in East Antarctic snowfall to Australian rainfall, *Communications Earth & Environment*, 3, ARTN
884 175

885 [10.1038/s43247-022-00502-w, 2022.](https://doi.org/10.1038/s43247-022-00502-w)
886 [Udy, D. G., Vance, T. R., Kiem, A. S., Holbrook, N. J., and Curran, M. A. J.: Links between Large Scale Modes](https://doi.org/10.1175/Jcli-D-20-0297.1)
887 [of Climate Variability and Synoptic Weather Patterns in the Southern Indian Ocean, Journal of Climate, 34, 883-](https://doi.org/10.1175/Jcli-D-20-0297.1)
888 [899, 10.1175/Jcli-D-20-0297.1, 2021.](https://doi.org/10.1175/Jcli-D-20-0297.1)
889 [van Dalum, C. T., van de Berg, W. J., van den Broeke, M. R., and van Tiggelen, M.: The surface mass balance](https://doi.org/10.5194/egusphere-2024-3728)
890 [and near-surface climate of the Antarctic ice sheet in RACMO2.4p1, EGUsphere, 2025, 1-40, 10.5194/egusphere-](https://doi.org/10.5194/egusphere-2024-3728)
891 [Van Dalum, C. T., Van De Berg, W. J., Gadde, S. N., Van Tiggelen, M., Van Der Drift, T., Van Meijgaard, E.,](https://doi.org/10.5194/egusphere-2024-3728, 2025.
892 <a href=)
893 [Van Ulf, L. H., and Van Den Broeke, M. R.: First results of the polar regional climate model RACMO2.4, The](https://doi.org/10.5194/tc-18-4065-2024)
894 [Cryosphere, 18, 4065-4088, 10.5194/tc-18-4065-2024, 2024.](https://doi.org/10.5194/tc-18-4065-2024)
895 [van de Berg, W. J., van den Broeke, M. R., Reijmer, C. H., and van Meijgaard, E.: Reassessment of the Antarctic](https://doi.org/10.1029/2005jd006495)
896 [surface mass balance using calibrated output of a regional atmospheric climate model, Journal of Geophysical](https://doi.org/10.1029/2005jd006495)
897 [Research: Atmospheres, 111, 10.1029/2005jd006495, 2006.](https://doi.org/10.1029/2005jd006495)
898 [Verfaillie, D., Pelletier, C., Goosse, H., Jourdain, N. C., Bull, C. Y. S., Dalaiden, Q., Favier, V., Fichefet, T., and](https://doi.org/10.1038/s43247-022-00458-x)
899 [Wille, J. D.: The circum-Antarctic ice-shelves respond to a more positive Southern Annular Mode with regionally](https://doi.org/10.1038/s43247-022-00458-x)
900 [varied melting, Communications Earth & Environment, 3, 139, ARTN 139](https://doi.org/10.1038/s43247-022-00458-x)
901 [Wang, S.: New record of explosive warmings in East Antarctica, Sci. Bull., 68, 129-132, 2023.](https://doi.org/10.1038/s43247-022-00458-x, 2022.
902 <a href=)
903 [Wang, S., Ding, M. H., Liu, G., Li, G. C., and Chen, W.: Blocking Events in East Antarctica: Impact on](https://doi.org/10.1175/Jcli-D-23-0419.1)
904 [Precipitation and their Association with Large-Scale Atmospheric Circulation Modes, Journal of Climate, 37,](https://doi.org/10.1175/Jcli-D-23-0419.1)
905 [1333-1345, 10.1175/Jcli-D-23-0419.1, 2024.](https://doi.org/10.1175/Jcli-D-23-0419.1)
906 [Wang, W., Shen, Y. Z., Chen, Q. J., and Wang, F. W.: Unprecedented mass gain over the Antarctic ice sheet](https://doi.org/10.1029/2022JD03788)
907 [between 2021 and 2022 caused by large precipitation anomalies, Environmental Research Letters, 18, 124012,](https://doi.org/10.1029/2022JD03788)
908 [ARTN 124012](https://doi.org/10.1029/2022JD03788)
909 [10.1088/1748-9326/ad0863, 2023.](https://doi.org/10.1088/1748-9326/ad0863)
910 [Wille, J. D., Favier, V., Gorodetskaya, I. V., Agosta, C., Kittel, C., Beeman, J. C., Jourdain, N. C., Lenaerts, J. T.](https://doi.org/10.1029/2020JD033788)
911 [M., and Codron, F.: Antarctic Atmospheric River Climatology and Precipitation Impacts, J Geophys Res-Atmos,](https://doi.org/10.1029/2020JD033788)
912 [126, ARTN e2020JD033788](https://doi.org/10.1029/2020JD033788)
913 [Wille, J. D., Alexander, S. P., Amory, C., Baiman, R., Barthélemy, L., Bergstrom, D. M., Berne, A., Binder, H.,](https://doi.org/10.1029/2020JD033788, 2021.
914 <a href=)
915 [Blanchet, J., Bozkurt, D., Bracegirdle, T. J., Casado, M., Choi, T., Clem, K. R., Codron, F., Datta, R., Di Battista,](https://doi.org/10.1175/Jcli-D-23-0175.1)
916 [S., Favier, V., Francis, D., Fraser, A. D., Fourré, E., Garreaud, R. D., Genton, C., Gorodetskaya, I., González-](https://doi.org/10.1175/Jcli-D-23-0175.1)
917 [Herrero, S., Heinrich, V. J., Hubert, G., Joos, H., Kim, S. J., King, J. C., Kittel, C., Landais, A., Lazzara, M.,](https://doi.org/10.1175/Jcli-D-23-0175.1)
918 [Leonard, G. H., Lieser, J. L., MacLennan, M., Mikolajczyk, D., Neff, P., Ollivier, I., Picard, G., Pohl, B., Ralph,](https://doi.org/10.1175/Jcli-D-23-0175.1)
919 [F. M., Rowe, P., Schlosser, E., Shields, C. A., Smith, I. J., Sprenger, M., Trusel, L., Udy, D., Vance, T., Walker,](https://doi.org/10.1175/Jcli-D-23-0175.1)
920 [C., Wever, N., and Zou, X.: The Extraordinary March 2022 East Antarctica "Heat" Wave. Part I: Observations](https://doi.org/10.1175/Jcli-D-23-0175.1)
921 [and Meteorological Drivers, Journal of Climate, 37, 757-778, 10.1175/Jcli-D-23-0175.1, 2024.](https://doi.org/10.1175/Jcli-D-23-0175.1)
922 [Williams, S. D. P., Moore, P., King, M. A., and Whitehouse, P. L.: Revisiting GRACE Antarctic ice mass trends](https://doi.org/10.1016/j.epsl.2013.10.016)
923 [and accelerations considering autocorrelation, Earth and Planetary Science Letters, 385, 12-21,](https://doi.org/10.1016/j.epsl.2013.10.016)
924 [Xin, M., Clem, K. R., Turner, J., Stammerjohn, S. E., Zhu, J., Cai, W., and Li, X.: West-warming East-cooling](https://doi.org/10.1016/j.epsl.2013.10.016, 2014.
925 <a href=)
926 [trend over Antarctica reversed since early 21st century driven by large-scale circulation variation, Environmental](https://doi.org/10.1088/1748-9326/acd8d4)
927 [Zhang, B., Yao, Y. B., Liu, L., and Yang, Y. J.: Interannual ice mass variations over the Antarctic ice sheet from](https://doi.org/10.1088/1748-9326/acd8d4, 2023.
928 <a href=)
929 [2003 to 2017 were linked to El Niño-Southern Oscillation, Earth and Planetary Science Letters, 560, 116796,](https://doi.org/10.1029/2017ea005696)
930 [ARTN 116796](https://doi.org/10.1029/2017ea005696)
931 [Arblaster, J. M. and Meehl, G. A.: Contributions of external forcings to southern annular mode trends, Journal of](https://doi.org/10.1029/2017ea005696, 2021.
932 <a href=)
933 [Climate, 19, 2896-2905, Dei 10.1175/Jcli3774.1, 2006.](https://doi.org/10.1175/Jcli-D-23-037859)
934 [Baiman, R., Winters, A. C., Lenaerts, J., and Shields, C. A.: Synoptic Drivers of Atmospheric River Induced](https://doi.org/10.1029/2022JD037859)
935 [Precipitation Near Dronning Maud Land, Antarctica, Journal of Geophysical Research \(Atmospheres\), 128,](https://doi.org/10.1029/2022JD037859)
936 [Bedard, J. A. and Bingham, R. J.: The Impact of the Extreme 2015-2016 El Niño on the Mass Balance of the](https://doi.org/10.1029/2022JD037859, 10.1029/2022JD037859, 2023.
937 <a href=)
938 [Antarctic Ice Sheet, Geophysical Research Letters, 46, 13862-13871, 10.1029/2019gl084466, 2019.](https://doi.org/10.1029/2012gl053316)
939 [Beening, C., Lebsoek, M., Landerer, F., and Stephens, G.: Snowfall driven mass change on the East Antarctic ice](https://doi.org/10.1029/2012gl053316)
940 [sheet, Geophysical Research Letters, 39, n/a-n/a, Artn L21501](https://doi.org/10.1029/2012gl053316)
941 [Cai, W. J., Santoso, A., Collins, M., Dewitte, B., Karamperidou, C., Kug, J. S., Lengaigne, M., McPhaden, M. J.,](https://doi.org/10.1029/2012gl053316, 2012.
942 <a href=)
943 [Stuecker, M. F., Taschetto, A. S., Timmermann, A., Wu, L. X., Yeh, S. W., Wang, G. J., Ng, B., Jia, F., Yang,](https://doi.org/10.1029/2012gl053316)
944 [Y., Ying, J., Zheng, X. T., Bayr, T., Brown, J. R., Capotondi, A., Cobb, K. M., Gan, B. L., Geng, T., Ham, Y. G.,](https://doi.org/10.1029/2012gl053316)

945 Jin, F. F., Jo, H. S., Li, X. C., Lin, X. P., McGregor, S., Park, J. H., Stein, K., Yang, K., Zhang, L., and Zhong, W. X.: Changing El Niño Southern Oscillation in a warming climate, *Nature Reviews Earth & Environment*, 2, 628–644, 10.1038/s43017-021-00199-z, 2021.

946 Chen, X. Y., Li, S. L., and Zhang, C.: Distinct impacts of two kinds of El Niño on precipitation over the Antarctic 947 Peninsula and West Antarctica in austral spring, *Atmospheric and Oceanic Science Letters*, 16, 100387, ARTN 948 100387, 10.1016/j.aosl.2023.100387, 2023.

949 Clem, K. R. and Fogt, R. L.: Varying roles of ENSO and SAM on the Antarctic Peninsula climate in austral spring, 950 *J Geophys Res Atmos*, 118, 11481–11492, 10.1002/2013JD020860, 2013.

951 Clem, K. R., Renwick, J. A., and McGregor, J.: Large Scale Forcing of the Amundsen Sea Low and Its Influence 952 on Sea Ice and West Antarctic Temperature, *Journal of Climate*, 30, 8405–8424, 10.1175/JCLI-D-16-0891.1, 2017.

953 Clem, K. R., Renwick, J. A., McGregor, J., and Fogt, R. L.: The relative influence of ENSO and SAM on Antarctic 954 Peninsula climate, *J Geophys Res Atmos*, 121, 9324–9341, 10.1002/2016JD025305, 2016.

955 Dahle, C., Murböck, M., Flechtner, F., Dobslaw, H., Michalak, G., Neumayer, K. H., Abrikosov, O., Reinhold, 956 A., König, R., Sulzbach, R., and Förste, C.: The GFZ GRACE RL06 Monthly Gravity Field Time Series: 957 Processing Details and Quality Assessment, *Remote Sensing*, 11, 2116, ARTN 2116, 10.3390/rs11182116, 2019.

958 Dahle, C., Boergens, E., Sasgen, I., Döhne, T., Reißland, S., Dobslaw, H., Kleemann, V., Murböck, M., König, R., 959 Dill, R., Sips, M., Sylla, U., Groh, A., Horwath, M., and Flechtner, F.: GravIS: mass anomaly products from 960 satellite gravimetry, 10.5194/essd-2024-347, 2024.

961 Diener, T., Sasgen, I., Agosta, C., Fuerst, J. J., Braun, M. H., Konrad, H., and Fettweis, X.: Acceleration of 962 Dynamic Ice Loss in Antarctica From Satellite Gravimetry, *Frontiers in Earth Science*, 9, ARTN 741789, 10.3389/feart.2021.741789, 2021.

963 Fogt, R. L. and Marshall, G. J.: The Southern Annular Mode: Variability, trends, and climate impacts across the 964 Southern Hemisphere, *WIREs Climate Change*, 11, 10.1002/wcc.652, 2020a.

965 Fogt, R. L. and Marshall, G. J.: The Southern Annular Mode: Variability, trends, and climate impacts across the 966 Southern Hemisphere, *Wiley Interdisciplinary Reviews Climate Change*, 11, ARTN e652, 10.1002/wcc.652, 2020b.

967 Fogt, R. L., Bromwich, D. H., and Hines, K. M.: Understanding the SAM influence on the South Pacific ENSO 968 teleconnection, *Climate Dyn.*, 36, 1555–1576, 2011.

969 Fogt, R. L., Jones, J. M., and Renwick, J.: Seasonal Zonal Asymmetries in the Southern Annular Mode and Their 970 Impact on Regional Temperature Anomalies, *Journal of Climate*, 25, 6253–6270, 10.1175/JCLI-D-11-00474.1, 971 2012.

972 Gardner, A. S., Moholdt, G., Scambos, T., Fahnestock, M., Ligtenberg, S., van den Broeke, M., and Nilsson, J.: 973 Increased West Antarctic and unchanged East Antarctic ice discharge over the last 7 years, *Cryosphere*, 12, 521–547, 10.5194/tc-12-521-2018, 2018.

974 Goyal, R., Jucker, M., Gupta, A. S., and England, M. H.: A New Zonal Wave 3 Index for the Southern 975 Hemisphere, *Journal of Climate*, 35, 5137–5149, 10.1175/JCLI-D-21-0927.1, 2022.

976 Groh, A. and Horwath, M.: The method of tailored sensitivity kernels for GRACE mass change estimates, April 977 01, 20162016.

978 Hersbach, H., Bell, B., Berrisford, P., Hirahara, S., Horányi, A., Muñoz-Sabater, J., Nicolas, J., Peubey, C., Radu, 979 R., Schepers, D., Simmons, A., Soci, C., Abdalla, S., Abellán, X., Balsamo, G., Bechtold, P., Biavati, G., Bidlot, 980 J., Bonavita, M., De Chiara, G., Dahlgren, P., Dee, D., Diamantakis, M., Dragani, R., Flemming, J., Forbes, R., 981 Fuentes, M., Geer, A., Haimberger, L., Healy, S., Hogan, R. J., Hólm, E., Janisková, M., Keeley, S., Laloyaux, 982 P., Lopez, P., Lupu, C., Radnoti, G., de Rosnay, P., Rozum, I., Vamborg, F., Villaume, S., and Thépaut, J. N.: 983 The ERA5 global reanalysis, *Quarterly Journal of the Royal Meteorological Society*, 146, 1999–2049, 10.1002/qj.3803, 2020.

984 Hosking, J. S., Orr, A., Marshall, G. J., Turner, J., and Phillips, T.: The Influence of the Amundsen Bellingshausen 985 Seas Low on the Climate of West Antarctica and Its Representation in Coupled Climate Model Simulations, 986 *Journal of Climate*, 26, 6633–6648, 10.1175/JCLI-D-12-00813.1, 2013.

987 Hoskins, B. J. and Karoly, D. J.: The Steady Linear Response of a Spherical Atmosphere to Thermal and 988 Orographic Forcing, *Journal of the Atmospheric Sciences*, 38, 1179–1196, Doi 10.1175/1520-9770(1981)038<1179:TSLRA>2.0.CO;2, 1981.

989 Huguenin, M. F., Holmes, R. M., Spence, P., and England, M. H.: Subsurface Warming of the West Antarctic 990 Continental Shelf Linked to El Niño Southern Oscillation, *Geophysical Research Letters*, 51, ARTN 991 e2023GL104518, 10.1029/2023GL104518, 2024.

992 Kim, B. H., Seo, K. W., Eom, J., Chen, J., and Wilson, C. R.: Antarctic ice mass variations from 1979 to 2017 993 driven by anomalous precipitation accumulation, *Sci Rep*, 10, 20366, 10.1038/s41598-020-77403-5, 2020.

994

995

996

997

998

999

000

001

002

003

004 Kim, B. H., See, K. W., Lee, C. K., Kim, J. S., Lee, W. S., Jin, E. K., and van den Broeke, M.: Partitioning the
005 drivers of Antarctic glacier mass balance (2003–2020) using satellite observations and a regional climate model,
006 *Proc Natl Acad Sci U S A*, 121, e2322622121, 10.1073/pnas.2322622121, 2024.

007 King, M. A. and Christoffersen, P.: Major Modes of Climate Variability Dominate Nonlinear Antarctic Ice Sheet
008 Elevation Changes 2002–2020, *Geophysical Research Letters*, 51, ARTN e2024GL108844
009 10.1029/2024GL108844, 2024.

010 King, M. A., Lyu, K., and Zhang, X. B.: Climate variability a key driver of recent Antarctic ice mass change,
011 *Nature Geoscience*, 16, 1128–1135, 10.1038/s41561-023-01317-w, 2023.

012 Landerer, F. W., Flechtner, F. M., Save, H., Webb, F. H., Bandikova, T., Bertiger, W. I., Bettadpur, S. V., Byun,
013 S. H., Dahle, C., Dobslaw, H., Fahnestock, E., Harvey, N., Kang, Z. G., Kruizinga, G. L. H., Loomis, B. D.,
014 McCullough, C., Murböck, M., Nagel, P., Paik, M., Pie, N., Poole, S., Strekalov, D., Tamisiea, M. E., Wang, F.
015 R., Watkins, M. M., Wen, H. Y., Wiese, D. N., and Yuan, D. N.: Extending the Global Mass Change Data Record:
016 GRACE Follow On Instrument and Science Data Performance, *Geophysical Research Letters*, 47, ARTN
017 e2020GL088306
018 10.1029/2020GL088306, 2020.

019 Lee, H. J., Jin, E. K., Kim, B. H., and Lee, W. S.: Vanishing of the El Niño induced delay effect on the ice mass
020 loss of West Antarctica in future climate change, 10.21203/rs.3.rs-2437498/v1, 2023.

021 Li, Z., Chao, B. F., Wang, H., and Zhang, Z.: Antarctica ice mass variations on interannual timescale: Coastal
022 Dipole and propagating transports, *Earth and Planetary Science Letters*, 595, 117789, ARTN 117789
023 10.1016/j.epsl.2022.117789, 2022.

024 Macha, J. M. A., Mackintosh, A. N., McCormack, F. S., Henley, B. J., McGregor, H. V., van Dalum, C. T., and
025 Purich, A.: Distinct Central and Eastern Pacific El Niño Influence on Antarctic Surface Mass Balance,
026 *Geophysical Research Letters*, 51, ARTN e2024GL109423
027 10.1029/2024GL109423, 2024.

028 Marshall, G. J.: Trends in the southern annular mode from observations and reanalyses, *Journal of Climate*, 16,
029 4134–4143, Doi 10.1175/1520-0442(2003)016<4134:TitSam>2.0.Co;2, 2003.

030 Marshall, G. J., Orr, A., and Turner, J.: A Predominant Reversal in the Relationship between the SAM and East
031 Antarctic Temperatures during the Twenty First Century, *Journal of Climate*, 26, 5196–5204, 10.1175/JCLI-D-12-
032 00671.1, 2013.

033 Marshall, G. J., Thompson, D. W. J., and van den Broeke, M. R.: The Signature of Southern Hemisphere
034 Atmospheric Circulation Patterns in Antarctic Precipitation, *Geophys. Res. Lett.*, 44, 11580–11589,
035 10.1002/2017GL075998, 2017.

036 McPhaden, M. J., Zebiak, S. E., and Glantz, M. H.: ENSO as an integrating concept in earth science, *Science*,
037 314, 1740–1745, 10.1126/science.1132588, 2006.

038 Medley, B. and Thomas, E. R.: Increased snowfall over the Antarctic Ice Sheet mitigated twentieth century sea-
039 level rise, *Nature Climate Change*, 9, 34+, 10.1038/s41558-018-0356-x, 2019.

040 Orr, A., Marshall, G. J., Hunt, J. C. R., Sommeria, J., Wang, C. G., Van Lipzig, N. P. M., Cresswell, D., and King,
041 J. C.: Characteristics of Summer Airflow over the Antarctic Peninsula in Response to Recent Strengthening of
042 Westerly Circumpolar Winds, *Journal of the Atmospheric Sciences*, 65, 1396–1413, 10.1175/2007jas2498.1,
043 2008.

044 Palóczy, A., Gille, S. T., and McClean, J. L.: Oceanic Heat Delivery to the Antarctic Continental Shelf: Large-
045 Scale, Low Frequency Variability, *Journal of Geophysical Research: Oceans*, 123, 7678–7701,
046 10.1029/2018JC014345, 2018.

047 Paolo, F. S., Padman, L., Fricker, H. A., Adusumilli, S., Howard, S., and Siegfried, M. R.: Response of Pacific-
048 sector Antarctic ice shelves to the El Niño/Southern Oscillation, *Nat Geosci*, 11, 121–126, 10.1038/s41561-017-
049 0033-0, 2018.

050 Pohl, B., Favier, V., Wille, J., Udy, D. G., Vanee, T. R., Pergaud, J., Dutrievoz, N., Blanchet, J., Kittel, C., Amory,
051 C., Krinner, G., and Codron, F.: Relationship Between Weather Regimes and Atmospheric Rivers in East
052 Antarctica, *Journal of Geophysical Research: Atmospheres*, 126, 10.1029/2021jd035294, 2021.

053 Peacock, M. J., McIntosh, P. C., and Meyers, G. A.: The Synoptic Decomposition of Cool Season Rainfall in the
054 Southeastern Australian Cropping Region, *Journal of Applied Meteorology and Climatology*, 45, 1156–1170,
055 10.1175/jam2394.1, 2006.

056 Raphael, M. N.: A zonal wave 3 index for the Southern Hemisphere, *Geophysical Research Letters*, 31, n/a–n/a,
057 ARTN L23212
058 10.1029/2004gl020365, 2004.

059 Raphael, M. N., Marshall, G. J., Turner, J., Fogt, R. L., Schneider, D., Dixon, D. A., Hosking, J. S., Jones, J. M.,
060 and Hobbs, W. R.: The Amundsen Sea Low: Variability, Change, and Impact on Antarctic Climate, *Bulletin of
061 the American Meteorological Society*, 97, 111–121, 10.1175/bams-d-14-00018.1, 2016a.

062 Raphael, M. N., Marshall, G. J., Turner, J., Fogt, R. L., Schneider, D., Dixon, D. A., Hosking, J. S., Jones, J. M.,
063 and Hobbs, W. R.: THE AMUNDSEN SEA LOW Variability, Change, and Impact on Antarctic Climate, *Bulletin*
064 *of the American Meteorological Society*, 97, 111–121, 10.1175/Bams-D-14-00018.1, 2016b.

065 Rayner, N. A., Parker, D. E., Horton, E. B., Folland, C. K., Alexander, L. V., Rowell, D. P., Kent, E. C., and
066 Kaplan, A.: Global analyses of sea surface temperature, sea ice, and night marine air temperature since the late
067 nineteenth century, *J Geophys Res Atmos*, 108, Artn 4407
068 10.1029/2002jd002670, 2003.

069 Richard Peltier, W., Argus, D. F., and Drummond, R.: Comment on “An Assessment of the ICE 6G–C (VM5a)
070 Glacial Isostatic Adjustment Model” by Purell et al, *Journal of Geophysical Research: Solid Earth*, 123, 2019–
071 2028, 10.1002/2016jb013844, 2018.

072 Rignot, E., Mouginot, J., Scheuchl, B., van den Broeke, M., van Wessem, M. J., and Morlighem, M.: Four decades
073 of Antarctic Ice Sheet mass balance from 1979–2017, *Proc Natl Acad Sci U S A*, 116, 1095–1103,
074 10.1073/pnas.1812883116, 2019.

075 Sasgen, I., Groh, A., and Horwath, M.: COST G GravIS RL01 ice mass change products, 2020.

076 Sasgen, I., Dobslaw, H., Martinec, Z., and Thomas, M.: Satellite gravimetry observation of Antarctic snow
077 accumulation related to ENSO, *Earth and Planetary Science Letters*, 299, 352–358, 10.1016/j.epsl.2010.09.015,
078 2010.

079 Searchilli, C., Frezzotti, M., and Ruti, P. M.: Snow precipitation at four ice core sites in East Antarctica:
080 provenance, seasonality and blocking factors, *Climate Dynamics*, 37, 2107–2125, 10.1007/s00382-010-0946-4,
081 2011.

082 Schneider, D. P., Okumura, Y., and Deser, C.: Observed Antarctic Interannual Climate Variability and Tropical
083 Linkages, *Journal of Climate*, 25, 4048–4066, 10.1175/Jcli-D-11-00273.1, 2012.

084 Shepherd, A., Ivins, E. R., A, G., Barletta, V. R., Bentley, M. J., Bettadpur, S., Briggs, K. H., Bromwich, D. H.,
085 Forsberg, R., Galin, N., Horwath, M., Jacobs, S., Joughin, I., King, M. A., Lenaerts, J. T., Li, J., Ligtenberg, S.
086 R., Luckman, A., Lutheke, S. B., McMillan, M., Meister, R., Milne, G., Mouginot, J., Muir, A., Nicolas, J. P.,
087 Paden, J., Payne, A. J., Pritchard, H., Rignot, E., Rott, H., Sorensen, L. S., Scambos, T. A., Scheuchl, B., Schrama,
088 E. J., Smith, B., Sundal, A. V., van Angelen, J. H., van de Berg, W. J., van den Broeke, M. R., Vaughan, D. G.,
089 Velicogna, I., Wahr, J., Whitehouse, P. L., Wingham, D. J., Yi, D., Young, D., and Zwally, H. J.: A reconciled
090 estimate of ice sheet mass balance, *Science*, 338, 1183–1189, 10.1126/science.1228102, 2012.

091 Shields, C. A., Wille, J. D., Marquardt Collow, A. B., MacLennan, M., and Gerodetskaya, I. V.: Evaluating
092 Uncertainty and Modes of Variability for Antarctic Atmospheric Rivers, *Geophysical Research Letters*, 49,
093 10.1029/2022gl099577, 2022.

094 Stevenson, S., Fox Kemper, B., Jochum, M., Rajagopalan, B., and Yeager, S. G.: ENSO Model Validation Using
095 Wavelet Probability Analysis, *Journal of Climate*, 23, 5540–5547, 10.1175/2010jcli3609.1, 2010.

096 Swenson, S., Chambers, D., and Wahr, J.: Estimating geocenter variations from a combination of GRACE and
097 ocean model output, *Journal of Geophysical Research Solid Earth*, 113, Artn B08410
098 10.1029/2007jb005338, 2008.

099 Tapley, B. D., Bettadpur, S., Ries, J. C., Thompson, P. F., and Watkins, M. M.: GRACE measurements of mass
100 variability in the Earth system, *Science*, 305, 503–505, 10.1126/science.1099192, 2004.

101 team, I.: Mass balance of the Antarctic Ice Sheet from 1992 to 2017, *Nature*, 558, 219–222, 10.1038/s41586-018-
102 0179-y, 2018.

103 Turner, J.: The El Niño southern oscillation and Antarctica, *International Journal of Climatology*, 24, 1–31,
104 10.1002/joc.965, 2004.

105 Turner, J., Phillips, T., Hosking, J. S., Marshall, G. J., and Orr, A.: The Amundsen Sea low, *International Journal*
106 *of Climatology*, 33, 1818–1829, 10.1002/joc.3558, 2012.

107 Turner, J., Orr, A., Gudmundsson, G. H., Jenkins, A., Bingham, R. G., Hillenbrand, C. D., and Bracegirdle, T. J.:
108 Atmosphere–ocean–ice interactions in the Amundsen Sea Embayment, West Antarctica, *Reviews of Geophysics*,
109 55, 235–276, 10.1002/2016rg000532, 2017.

110 Udy, D. G., Vane, T. R., Kiem, A. S., and Holbrook, N. J.: A synoptic bridge linking sea salt aerosol
111 concentrations in East Antarctic snowfall to Australian rainfall, *Communications Earth & Environment*, 3, ARTN
112 175
113 10.1038/s43247-022-00502-w, 2022.

114 Udy, D. G., Vane, T. R., Kiem, A. S., Holbrook, N. J., and Curran, M. A. J.: Links between Large Scale Modes
115 of Climate Variability and Synoptic Weather Patterns in the Southern Indian Ocean, *Journal of Climate*, 34, 883–
116 899, 10.1175/Jcli-D-20-0297.1, 2021.

117 van Dalum, C. T., van de Berg, W. J., van den Broeke, M. R., and van Tiggelen, M.: The surface mass balance
118 and near surface climate of the Antarctic ice sheet in RACMO2.4p1, *EGUsphere*, 2025, 1–40, 10.5194/egusphere-
119 2024-3728, 2025.

120 [Van Dalum, C. T., Van De Berg, W. J., Gadde, S. N., Van Tiggelen, M., Van Der Drift, T., Van Meijgaard, E.,](#)
121 [Van Ulft, L. H., and Van Den Broeke, M. R.: First results of the polar regional climate model RACMO2.4, The](#)
122 [Cryosphere, 18, 4065–4088, 10.5194/tc-18-4065-2024, 2024.](#)

123 [van de Berg, W. J., van den Broeke, M. R., Reijmer, C. H., and van Meijgaard, E.: Reassessment of the Antarctic](#)
124 [surface mass balance using calibrated output of a regional atmospheric climate model, Journal of Geophysical](#)
125 [Research: Atmospheres, 111, 10.1029/2005jd006495, 2006.](#)

126 [Verfaillie, D., Pelletier, C., Goosse, H., Jourdain, N. C., Bull, C. Y. S., Dalaiden, Q., Favier, V., Fichefet, T., and](#)
127 [Wille, J. D.: The circum Antarctic ice shelves respond to a more positive Southern Annular Mode with regionally](#)
128 [varied melting, Communications Earth & Environment, 3, 139, ARTN 139](#)
129 [10.1038/s43247-022-00458-x, 2022.](#)

130 [Wang, S.: New record of explosive warmings in East Antarctica, Sci. Bull., 68, 129–132, 2023.](#)

131 [Wang, S., Ding, M. H., Liu, G., Li, G. C., and Chen, W.: Blocking Events in East Antarctica: Impact on](#)
132 [Precipitation and their Association with Large Scale Atmospheric Circulation Modes, Journal of Climate, 37,](#)
133 [1333–1345, 10.1175/JCLI-D-23-0419.1, 2024.](#)

134 [Wang, W., Shen, Y. Z., Chen, Q. J., and Wang, F. W.: Unprecedented mass gain over the Antarctic ice sheet](#)
135 [between 2021 and 2022 caused by large precipitation anomalies, Environmental Research Letters, 18, 124012,](#)
136 [ARTN 124012](#)
137 [10.1088/1748-9326/ad0863, 2023.](#)

138 [Wille, J. D., Favier, V., Gorodetskaya, I. V., Agosta, C., Kittel, C., Beaman, J. C., Jourdain, N. C., Lenaerts, J. T.](#)
139 [M., and Codron, F.: Antarctic Atmospheric River Climatology and Precipitation Impacts, J Geophys Res Atmos,](#)
140 [126, ARTN e2020JD033788](#)
141 [10.1029/2020JD033788, 2021.](#)

142 [Wille, J. D., Alexander, S. P., Amory, C., Baiman, R., Barthélemy, L., Bergstrom, D. M., Berne, A., Binder, H.,](#)
143 [Blanchet, J., Bozkurt, D., Bracegirdle, T. J., Casade, M., Choi, T., Clem, K. R., Codron, F., Datta, R., Di Battista,](#)
144 [S., Favier, V., Francis, D., Fraser, A. D., Fourré, E., Garreaud, R. D., Genton, C., Gorodetskaya, I., González-](#)
145 [Herrero, S., Heinrich, V. J., Hubert, G., Jees, H., Kim, S. J., King, J. C., Kittel, C., Landais, A., Lazzara, M.,](#)
146 [Leonard, G. H., Lieser, J. L., MacLennan, M., Mikolajczyk, D., Neff, P., Ollivier, I., Picard, G., Pohl, B., Ralph,](#)
147 [F. M., Rowe, P., Schlosser, E., Shields, C. A., Smith, I. J., Sprenger, M., Trusel, L., Udy, D., Vance, T., Walker,](#)
148 [C., Wever, N., and Zou, X.: The Extraordinary March 2022 East Antarctica "Heat" Wave. Part I: Observations](#)
149 [and Meteorological Drivers, Journal of Climate, 37, 757–778, 10.1175/JCLI-D-23-0175.1, 2024.](#)

150 [Williams, S. D. P., Moore, P., King, M. A., and Whitehouse, P. L.: Revisiting GRACE Antarctic ice mass trends](#)
151 [and accelerations considering autocorrelation, Earth and Planetary Science Letters, 385, 12–21,](#)
152 [https://doi.org/10.1016/j.epsl.2013.10.016, 2014.](https://doi.org/10.1016/j.epsl.2013.10.016)

153 [Xin, M., Clem, K. R., Turner, J., Stammerjohn, S. E., Zhu, J., Cai, W., and Li, X.: West warming East cooling](#)
154 [trend over Antarctica reversed since early 21st century driven by large scale circulation variation, Environmental](#)
155 [Research Letters, 18, 064034, 10.1088/1748-9326/acd8d4, 2023.](#)

156 [Zhang, B., Yao, Y. B., Liu, L., and Yang, Y. J.: Interannual ice mass variations over the Antarctic ice sheet from](#)
157 [2003 to 2017 were linked to El Niño Southern Oscillation, Earth and Planetary Science Letters, 560, 116796,](#)
158 [ARTN 116796](#)
159 [10.1016/j.epsl.2021.116796, 2021.](#)

160